Atomic Data and Nuclear Data Tables **79,** 143–184 (2001)
doi:10.1006/adnd.2001.0866, available online at http://www.idealibrary.com on IDEAL®

ANALYTIC CROSS SECTIONS FOR ELECTRON COLLISIONS WITH CO, CO_2, AND H_2O RELEVANT TO EDGE PLASMA IMPURITIES

TOSHIZO SHIRAI

Department of Nuclear Energy Systems, Japan Atomic Energy Research Institute, Tokai-mura, Ibaraki 319-1195, Japan

TATSUO TABATA

Osaka Prefecture University, Gakuen-cho, Sakai, Osaka 599-8531, Japan,
and Institute for Data Evaluation and Analysis, Kami, Sakai, Osaka 593-8311, Japan

and

HIROYUKI TAWARA

Physics Department, Kansas State University, Manhattan, Kansas 66506-2604

Cross section data in the energy range above 1 eV have been critically evaluated for electron impact collision processes involving the impurity species (CO, CO_2, and H_2O) most relevant to low-temperature plasmas. A short review of the cross section measurements is given for each collision process. The literature has been surveyed up to December 1999. Analytic fits to the recommended cross sections are also presented. © 2001 Academic Press

0092-640X/01 $35.00

CONTENTS

INTRODUCTION 144
Data Sources 144
Carbon Monoxide Molecule 144
Carbon Dioxide Molecule 146
Water Molecule 147
Analytic Expressions 149
EXPLANATION OF TABLES 153
EXPLANATION OF GRAPHS 153
TABLES
I. Energy Ranges of Data, Fitting Errors, and Parameters of the Analytic Expressions for CO 154
II. Energy Ranges of Data, Fitting Errors, and Parameters of the Analytic Expressions for CO_2 158
III. Energy Ranges of Data, Fitting Errors, and Parameters of the Analytic Expressions for H_2O 160
GRAPHS
Cross Section vs Electron Energy 162

INTRODUCTION

The atomic and molecular data for collision processes involving electron impact on CO, CO_2, and H_2O are not only of astrophysical interest but also important for practical applications such as the modeling of various discharge, plasma, and laser systems.

Two compilations of cross section data for CO have been available up to now. One is by Kanik et al. [1], who derived recommended data from experimental measurements for total and elastic scattering, vibrational excitation, and total ionization. The other is on the cross sections for vibrational excitation, electronic excitation, dissociation, and ionization, by Liu and Victor [2]. For electronic excitation they additionally made use of theoretical calculations.

The present compilation is based on experimental data sets except for the recommended data of Ref. [1] with a slight revision based on recent measurements for vibrational excitation. All relevant papers published through December 1999 were collected and surveyed, and the best measured data for various processes in our judgment, based on consistency check or experimental uncertainty, have been plotted in separate graphs. In cases where only a single measurement is available, we have adopted it as the recommended value. In some cases where there exist large variations among different measurements, we have renormalized the data sets to the most reliable one in order to extend our recommended data set across as wide an energy range as possible.

In order to facilitate the input of numerical data for practical applications, we also present analytical least-squares fits to all the recommended data sets reported here.

Data Sources

Carbon Monoxide Molecule

Total scattering. Measurements of total cross section were carried out by García et al. [3] in the energy range 380–5200 eV and by Kanik et al. [4] in the range 5–300 eV using a beam attenuation technique. Kanik et al. [1] critically reviewed earlier measurements and recommended a data set in the energy range 1–1000 eV. We have adopted their recommended data set in this energy range, and at impact energies above 1000 eV, we adopted the values of García et al. [3] as quoted in Ref. [1]. More recently, Karwasz et al. [5] remeasured the cross sections in the energy range 80–4000 eV with a statistical error of $\pm 3\%$ using a modified

Ramsauer-type electron spectrometer. Their cross sections fall off more rapidly at high energies than the present recommended data set (Graph 1).

Elastic scattering. Kanik et al. [1] provided recommended cross sections for elastic scattering; the data set is plotted here (Graph 2) along with a recent crossed-beam measurement by Gibson et al. [6] having an estimated uncertainty of ±15% in the energy range 1–30 eV.

Momentum transfer cross sections (Graph 3) with an estimated uncertainty of ±30% in the energy range 3–100 eV have been taken from Gibson et al. [6] and from Tanaka et al. [7]. These two measurements join smoothly. In order to make the extrapolation reliable, we have also utilized the results of Land [8] and Haddad and Milloy [9] at energies below 1 eV and a critical compilation by Itikawa [10] at energies above 100 eV.

Vibrational excitation. Kanik et al. [1] provided recommended data for the $v = 0 \rightarrow 1$ transition. The second peak at 20 eV is about an order of magnitude smaller than that in the new data of Gibson et al. [6]. We have adopted these new results in the energy range 1–30 eV (Graph 4). The uncertainty is estimated to be ±20%.

Electronic excitation. Kanik et al. [1] deduced the total cross section for electronic excitation to all accessible states by subtracting the ionization, elastic scattering, and vibrational excitation cross sections from the total scattering cross section. The vibrational excitation cross sections adopted here (Graph 5) essentially coincide with their recommended data set.

Vibronic excitation. Mumma et al. [11] measured the relative cross sections for excitation to the ($A\ ^1\Pi; v = 0, 1, 2, 3, 4$) bands in the energy range from threshold to 350 eV. These data were put on an absolute scale by normalizing to the cross section for production of Lyman-α radiation by dissociative excitation of H_2 at 300 eV. The uncertainty is estimated to be ±13%. Cross sections for all values of v show a similar energy dependence with a maximum at around 30 eV. We have adopted these Mumma et al. values (Graphs 6–10). Cross sections summed over $v = 0$–4 were also reported by Zobel et al. [12] and Zetner et al. [13] in the narrow energy range from threshold to 15 eV. The cross section value of Ref. [13] at 15 eV is about 50% larger than the corresponding value of Ref. [11], which is almost equal to the emission cross sections summed over all vibrational states (see Graph 20). Therefore we have omitted these data sets. Wells et al. [14] and Manson and Newell [15] measured the cross sections for excitation to the $I\ ^1\Sigma^-$ state (Graph 11). Kanik et al. [16] measured the cross sections for excitation to the $B\ ^1\Sigma^+$ (Graph 12) and $C\ ^1\Sigma^+$ (Graph 13) states at 100 eV impact energy by using electron energy-loss spectroscopy. The experimental uncertainty is estimated to be ±26%. To estimate the excitation cross sections at other impact energies, we have assumed the energy dependence to be identical to the respective emission cross sections corresponding to the transitions from the ($B\ ^1\Sigma^+; v = 0$) and ($C\ ^1\Sigma^+; v = 0$) bands to the ground ($X\ ^1\Sigma^+; v = 0$) band (see Graphs 17 and 18). Kanik et al. [16] also reported an absolute cross section of 4.43×10^{-18} cm^2 for excitation to the ($E\ ^1\Pi; v = 0$) band at 100 eV. This value was used by Ciocca et al. [17] to normalize the excitation function they measured. Using analytic fits of the form of a modified Born-approximation equation, they derived a data set adopted here (Graph 14).

Cross sections for excitation to the triplet $a\ ^3\Pi$ state were measured by LeClair et al. [18], Zobel et al. [12], Furlong and Newell [19], and Zetner et al. [13]. Except for the data set of Ref. [18] adopted here (Graph 15), all other results fall off steeply compared with the emission cross sections for the Cameron band (see Graph 21). Excitation cross sections to the $a'\ ^3\Sigma^+$ and $d\ ^3\Delta$ states are also available in Refs. [12, 13]. However, we have omitted them because the measured energy range is too narrow.

Emission from CO.* The relative emission cross sections for the bands of ($A\ ^1\Pi$–$X\ ^1\Sigma^+; v = 0$–1) at 1597 Å, ($B\ ^1\Sigma^+$–$X\ ^1\Sigma^+; v = 0$–0) at 1150 Å, and ($C\ ^1\Sigma^+$–$X\ ^1\Sigma^+; v = 0$–0) at 1088 Å for excited CO molecules were measured by Aarts and de Heer [20] in the energy range 0.1–5 keV. These data were normalized at 500 eV to the data of Lassettre and co-workers [21]. Mumma et al. [11] remeasured the cross sections corresponding to the first emission band and reported results in good agreement with those of Ref. [20] in the overlapping energy range 100–200 eV (Graph 16). A remeasurement with a resolution of 0.25 Å was recently reported by Kanik et al. [22] for the ($B\ ^1\Sigma^+$–$X\ ^1\Sigma^+; v = 0$–0) and ($C\ ^1\Sigma^+$–$X\ ^1\Sigma^+; v = 0$–0) emission bands at impact energies of 20, 100, and 200 eV. Their relative cross sections were put on an absolute scale by normalizing, at 200 eV, to the emission cross section of the 833.8 Å O II line, which was determined by James et al. [23] with a low spectral resolution of 5 Å. The uncertainty of the cross sections is estimated to be ±25%. For the ($B\ ^1\Sigma^+$–$X\ ^1\Sigma^+; v = 0$–0) emission band, the results of Refs. [20] and [22] agree well with each other (Graph 17). On the other hand, the result of Ref. [20] for the ($C\ ^1\Sigma^+$–$X\ ^1\Sigma^+; v = 0$–0) band had to be reduced by a factor of about 1.8 to fit that of Ref. [22] (Graph 18). Ciocca et al. [17] performed measurements of the ($E\ ^1\Pi$–$X\ ^1\Sigma^+; v = 0$–0) emission spectra at 30, 75, and 100 eV electron impact with a high resolution of 0.036 Å. They also

determined the absolute value of the emission cross section at 100 eV of 0.47×10^{-18} cm^2. The ratio of emission cross section to excitation cross section is about 10%. Our recommended data set has been derived from their analytic fit for the excitation cross section based on a modified Born equation (Graph 19).

Ajello [24] measured the relative cross sections for the ($A\ ^1\Pi$–$X\ ^1\Sigma^+$) band system in the wavelength range of 1270–2000 Å (Graph 20) and estimated their absolute values by normalizing to the cross sections of the $v = 0$–1 band measured by Aarts and de Heer [20]. It was found that the emission for $v = 0$–1 is only a few percent of the total band emission.

The cross sections for the spin-forbidden Cameron band ($a\ ^3\Pi$–$X\ ^1\Sigma^+$; $v = 1$–4) at 2389 Å were measured by Ajello [24]. The cross section values have been renormalized to that at 11 eV (maximum) of Erdman and Zipf [25] who corrected for the lifetime and admixture of other transitions (Graph 21).

Ionization. Single ionization cross sections were measured by Hille and Märk [26] with a double-focusing mass spectrometer and by Freund et al. [27] using a crossed-beam technique. Hille and Märk [26] also reported double ionization cross sections. Dissociative ionization cross sections for C^+ and O^+ production were measured by Orient and Srivastava [28] with a quadrupole mass spectrometer. A recent extensive measurement with a time-of-flight spectrometer was made by Tian and Vidal [29] for the cross sections for total, partial, and dissociative ionization in the energy range from threshold to 600 eV with an uncertainty of ±10%. Their results are adopted here (Graphs 22–28).

The total ionization cross sections adopted here (Graph 22) are also compared with the calculation based on the binary-encounter-Bethe model by Hwang et al. [30].

Ionization excitation to CO^{+*}. Cross sections for ionization excitation to the $A\ ^2\Pi$ and $B\ ^2\Sigma^+$ band systems were first measured by Skubenich [31] in the energy range from threshold to 150 eV. Aarts and de Heer [32] remeasured these cross sections with estimated uncertainties of ±11% and ±20%, respectively, in the energy range 50–5000 eV. We have renormalized the cross sections of Ref. [31] to those of Ref. [32], because the former are more than an order of magnitude smaller than the latter (Graphs 30 and 31).

Aarts and de Heer [32] also derived the cross section for ionization to the ground $X\ ^2\Sigma^+$ band system in the energy range 50–1000 eV (Graph 29) by subtraction of the $A\ ^2\Pi$ and $B\ ^2\Sigma^+$ cross sections from the single ionization cross section estimated from earlier measurements for total and dissociative ionization, which is in fairly good agreement with the present recommended data.

Emission from CO^{+*}. The cross sections for the two emission bands of ($A\ ^2\Pi$–$X\ ^2\Sigma^+$; $v = 3$–0) at 4011 Å (Graph 32) and ($B\ ^2\Sigma^+$–$X\ ^2\Sigma^+$; $v = 0$–0) at 2190 Å (Graph 33) were given by Aarts and de Heer [32] in the energy range 50–5000 eV. The uncertainties are estimated to be ±11% and ±20% for these two bands, respectively. The former emission band was remeasured by Ajello [24] at energy range below 300 eV. Both results agree with each other within an uncertainty of ±15%. Ajello [24] also reported the total emission cross sections for the ($A\ ^2\Pi$–$X\ ^2\Sigma^+$) (Graph 34) and ($B\ ^2\Sigma^+$–$X\ ^2\Sigma^+$) (Graph 35) band systems. The ratios of $v = 3$–0 and $v = 0$–0 band emission to total emission are 12% and 37%, respectively.

Dissociation. The cross section for dissociation to form the excited state atoms of C(^3P) and O(^3P) was first measured by Cosby [33] at impact energies from threshold to 198.5 eV (Graph 36). The experimental uncertainty is estimated to be ±26%. The cross section for O(^1S) production was provided by LeClair et al. [18] in the energy range from threshold to 500 eV (Graph 37) with an uncertainty of ±36%.

Emission from C^*, O^*, C^{+*}, and O^{+*}. Aarts and de Heer [20] measured the emission cross sections in the energy range 100–5000 eV for the following transitions: C I($2p3d\ ^3D^o, ^3F^o, 2p4s\ ^3P^o \rightarrow 2p^2\ ^3P$) at 1278–1280 Å (Graph 38), O I($2p^3 3s\ \ ^3S^o \rightarrow 2p^4\ \ ^3P$) at 1304 Å (Graph 39), and C II($2s2p^2\ ^2D \rightarrow 2s^2 2p\ ^2P^o$) at 1335 Å (Graph 40). Ajello [24] measured the same emission cross sections at low energies from threshold to 300 eV. Agreement between the two measurements in the overlapping energy region seems to be good. The emission cross section at 1304 Å was also measured by Lawrence [34] in addition to that for the O I($2p^3 3p\ ^3P \rightarrow 2p^3 3s\ ^3S^o$) transition at 8447 Å (Graph 41).

James et al. [23] identified a number of emission lines induced by electron impact at 20 and 200 eV over the wavelength range 480–1200 Å and reported the respective emission cross sections of the atomic dissociation fragments.

Carbon Dioxide Molecule

Total scattering. Total cross sections (Graph 42) were measured by Hoffman et al. [35], Kwan et al. [36], and Sueoka and Mori [37]. Later, extensive measurements were made by Szmytkowski et al. [38] and Garcia and Manero [39] in the energy ranges 0.5–3000 and 400–5000 eV, respectively. The experimental uncertainty of Ref. [38], where an attenuation method was employed for the energy range below 80 eV and

a modified Ramsauer technique above 60 eV, is estimated to be ±6%. The measurement in Ref. [39], made using an attenuation technique, has an estimated uncertainty of ±3%.

Elastic scattering. The elastic scattering (Graph 43) and momentum transfer (Graph 44) cross sections were measured by Register et al. [40] in the energy range 4–50 eV and by Iga et al. [41, 42] in the high energy region 100–1000 eV with an estimated uncertainty of ±20%. Tanaka et al. [43] reported both cross sections in the energy range 1.5–100 eV. The uncertainty is estimated to be ±50%. Recently, Gibson et al. [44] remeasured the corresponding cross sections over 1–50 eV with an estimated uncertainty of ±25%. Their elastic scattering cross section is systematically smaller by about 15% than that of Ref. [43] in the whole overlapping energy range. Their results have been adopted only in the energy range below 3 eV.

A swarm experiment of Nakamura [45] is available for the momentum transfer cross section data below 100 eV. His data agree well with the result of Ref. [44].

Ionization. A measurement for the single and double ionization cross sections using a double-focusing mass spectrometer was performed by Märk and Hille [46]. Crossed-beam measurements for the single ionization cross section were also reported by Freund et al. [27] and Krishnakumar [47].

A more extensive and accurate measurement using a time-of-flight mass spectrometer was carried out by Straub et al. [48] for total, partial, and dissociative ionization in the energy range from threshold to 1000 eV. The experimental uncertainty is estimated to be ±10%. A similar measurement was performed by Tian and Vidal [49] in the energy range up to 300 eV. The two sets of results are in good agreement. In addition these authors have also reported the absolute cross sections for different ion-pair and ion-neutral dissociative channels in single to quadruple ionization [50]. In the present compilation we have adopted the data sets for total (Graph 45) and partial (Graphs 46 and 53) ionization, and the data sets of dissociative channels in single ionization (Graphs 47–52) and in double ionization (Graphs 54–58). Cross sections for other dissociative channels are small, being on the order of 10^{-19} cm^2 or less.

The total ionization cross section adopted here is also compared with the calculation based on the binary-encounter-Bethe model by Hwang et al. [30] (Graph 45).

Emission from CO_2^+. The emission cross sections for the ($A\,^2\Pi_u$–$X\,^2\Pi_g$) (Graph 59) and ($B\,^2\Sigma_u^+$–$X\,^2\Pi_g$) (Graph 60) band systems in the wavelength ranges 2930–4390 and 2880–2900 Å, respectively, were measured by McConkey et al. [51], Ajello [52], and Tsurubuchi and Iwai [53]. For the latter band system, in Ref. [51] the cross section values multiplied by a factor of 2 are plotted, as was noted by Mentall et al. [54]. Though the three measurements agree with each other at high energies, some discrepancies are clearly seen at low energies. We have adopted the results of Refs. [51, 53].

Dissociative excitation. The relative cross sections for CO($A\,^1\Pi; v = 0, 1, 2, 3, 4$) production were measured by Mumma et al. [11] in the energy range below 350 eV. These data were put on an absolute scale by normalizing to the Lyman-α cross section at 300 eV. We have plotted the data only for the cases of $v = 0$ (Graph 61) and $v = 3$ (Graph 62), which are almost indistinguishable from those for $v = 1$ and 2 and for $v = 4$, respectively. The total cross section summed over these five vibrational levels reaches a maximum of 2.6×10^{-18} cm^2 at an energy near 40 eV. The experimental uncertainty is estimated to be ±17%.

Emission from CO. Ajello [52] measured the cross sections for the ($A\,^1\Pi$–$X\,^1\Sigma^+$) band system in the wavelength range 1350–1730 Å (Graph 63) and the ($a\,^3\Pi$–$X\,^1\Sigma^+$; $v = 0$–1) band at 2158 Å (Graph 64). It is noted that the relative cross section for the latter band is renormalized at 80 eV to the recent absolute value of Erdman and Zipf [25].

Emission from CO^+. Ajello [52] measured the cross section for the ($B\,^2\Sigma^+$–$X\,^2\Sigma^+$) band system in the wavelength range 2040–2510 Å (Graph 65).

Dissociation. The cross section for dissociation to form O(^1S) (Graph 66) was measured by LeClair and McConkey [55] at impact energies up to 1000 eV by using a pulsed crossed-beam method in combination with time-of-flight spectroscopy. The experimental uncertainty is estimated to be ±12%.

Emission from C^*, O^*, C^{+*}, O^{+*}, and O^{2+*}. Ajello [52] measured the cross sections for C I ($2p3d\,^3D^o$, $^3F^o$, $2p4s\,^3P^o - 2p^2\,^3P$) multiplets at 1278–1280 Å (Graph 67), O I ($2p^3 3s\,^3S^o - 2p^4\,^3P$) at 1304 Å (Graph 68), and C II ($2s2p^2\,^2D - 2s^2 2p\,^2P^o$) at 1335 Å (Graph 69) in the energy region below 300 eV.

The extreme ultraviolet emission spectrum induced by electron impact at 200 eV was identified by Kanik et al. [56] with a resolution of 5 Å over the wavelength range 480–1250 Å. Absolute cross sections were reported for each of 36 identified features for the atomic dissociation fragments.

Water Molecule

Total scattering. Measurements of the total scattering cross section (Graph 70) have been reported by Brüche [57], Sueoka et al. [58], Szmytkowski [59], Zecca et al. [60], and

Nishimura and Yano [61]. A recent remeasurement was carried out by Sağlam and Aktekin [62] with uncertainties ranging from ±1.3 to ±8.3% in the incident energy range 4–20 eV using an attenuation method. All the measurements except for Ref. [58] agree well.

Elastic scattering. Elastic scattering (Graph 71) and momentum transfer (Graph 72) cross sections were measured by Danjo and Nishimura [63], Katase et al. [64], and Shyn and Cho [65]. Two recent measurements have been reported. One is by Johnstone and Newell [66] in the impact energy range 6–50 eV; the experimental uncertainties for the two processes are ±20% and ±25%, respectively. The other is by Shyn and Grafe [67], in the energy range 30–200 eV with an estimated uncertainty of ±10%, using a modulated crossed-beam method. All the measurements are in good agreement except for Ref. [63] whose data are too low compared with the results of other measurements.

A critical compilation was reported by Hayashi [68] for the momentum transfer cross section data over a wide energy range. We have used his recommended data at low energies.

Vibrational excitation. The cross sections for the bending (010) (Graph 73) and stretching (100, 001) (Graph 74) modes were measured by Seng and Linder [69] in the energy range from threshold to 10 eV with an uncertainty of ±25%, using a crossed-beam method. They observed a strong and sharp threshold resonance as well as a broad resonance centered around 6–8 eV. A similar measurement was reported by Shyn et al. [70] in the energy range from 2.2 to 20 eV with an uncertainty of ±20%.

Ionization. Total, partial, and dissociative ionization cross sections (Graphs 75–81) were measured by Schutten et al. [71] in the energy range 20–2000 eV with an uncertainty of ±15%. Djurić et al. [72] observed only the total ionization cross section in the lower energy range of 15–150 eV. Both results were obtained using condenser plate techniques. A recent measurement using time-of-flight mass spectroscopy was carried out by Straub et al. [73], who reported the cross sections with uncertainties of ±4.5% for total ionization (Graph 75), of ±5.0% for H^+ production (Graph 81), and of ±11.5% for H_2^+ production (Graph 80) and O^{2+} production (Graph 79). The recommended cross sections for the production of H_2O^+ (Graph 76), OH^+ (Graph 77), and O^+ (Graph 78) ions have been taken from the measurement of Schutten et al. [71]. Summation of these cross sections is consistent with the corresponding partial ionization values given in Ref. [73] within 10%.

The recommended total ionization cross section is also compared with the calculation by Hwang et al. [30] based on the binary-encounter Bethe model (Graph 75).

Dissociative excitation. The cross sections for formation of excited H($n = 3, 4$) atoms (Graphs 82, 83) were given by Ogawa et al. [74] for an electron impact energy range of 50–1000 eV.

Emission from H.* Möhlmann et al. [75] determined the absolute cross section for Lyman-α radiation in the energy range from 17 eV to 2000 eV by normalizing their relative value at 100 eV to the value 1.2×10^{-17} cm^2 of Mumma and Zipf [76] for the case of electron impact on H_2. Recently, Tawara et al. [77] recommended a value of 7.3×10^{-18} cm^2 for this cross section. Therefore, values from Ref. [75] multiplied by a factor of 0.6 have been plotted here (Graph 84). The corrected values are in general agreement with earlier measurements not shown here.

The cross section for Balmer-α radiation was measured by Möhlmann and de Heer [78] in the electron impact-energy range 20–2000 eV with an estimated uncertainty of ±12%. We have quoted their result (Graph 85). They also reported the cross sections for Balmer radiation up to $n = 9$ at 100 eV impact energy with uncertainties ranging from ±12% (for $n = 4$) to ±30% (for $n \geq 5$). The Balmer-β emission cross sections recommended here (Graph 86) have been taken from Beenakker et al. [79], who also reported the cross sections for other Balmer radiation up to $n = 5$ at 300 eV. It is found that the emission yields of Balmer-α and Balmer-β radiation due to dissociative excitation to the $n = 3, 4$ states (see Graphs 82 and 83) are 56 and 45%, respectively. The cross sections for Balmer-γ and -δ emission were provided by Vroom and de Heer [80] in the energy range 50–6000 eV. In Graphs 87 and 88, we plot their data reduced by about 30% to fit the results of Refs. [78, 79].

A recent measurement was made by Müller et al. [81] for Balmer series radiation at 100 eV impact energy with a crossed-beam plus static gas-target method. It is noted that their results for Balmer-α and -β and Balmer-γ are about 25% and 30%, respectively, lower than the present recommended data sets.

Emission from OH. Sushanin and Kishko [82] measured the cross section for the $A\ ^2\Sigma^+ – X\ ^2\Pi$ band with $\delta v = 0$ at 3064 Å in the energy range below 70 eV. Their result is 4.1×10^{-19} cm^2 at 300 eV, which is about 20 times lower than that of Beenakker et al. [79] in the energy range 40–1000 eV. The values adopted from Ref. [82] are renormalized to those of Beenakker et al. [79] (Graph 89).

A recent measurement by Müller et al. [81] shows a cross section value at 100 eV of 2.68×10^{-18} cm^2. This value is about 40% smaller than the 4.64×10^{-18} cm^2 of Beenakker et al. [79] adopted here.

Emission from O I. Lawrence [34] measured the cross section for dissociative excitation to the $(2p^3 3s\ ^3S^o –$

$2p^4\ ^3P$) multiplet at 1304 Å. The cross section adopted is from a remeasurement of Morgan and Mentall [83] (Graph 90). These two data sets agree well with each other within the experimental uncertainty of ±20%. The emissions from the ($2p^3 3p\ ^5P - 2p^3 3s\ ^5S^o$) multiplet at 7774 Å (Graph 91) and from ($2p^3 3p\ ^3P - 2p^3 3s\ ^3S^o$) at 8447 Å (Graph 92) were observed by Beenakker et al. [79] in the energy range 40–1000 eV. We have adopted these cross sections. The latter multiplet was also measured by Lawrence [34], whose result agrees with that of Beenakker et al. [79] within the uncertainties of ±20% claimed in both experiments.

Analytic Expressions

The functional forms of the analytic expressions used for cross sections except for ionization cross sections are basically those semiempirically developed by Green and McNeal [84] and modifications of them such as used in our previous work [85, 86]. For ionization cross sections, the function with the asymptotic behavior of $\ln E/E$ (E is the incident electron energy) as proposed by Lotz [87] was used with a new factor to reproduce the behavior near threshold [see Eq. (10) below]. The relevant basic relations and definitions are as follows:

$$f_1(x; c_1, c_2) = \sigma_0 c_1 (x/E_R)^{c_2} \quad \text{(i)}$$

$$f_2(x; c_1, c_2, c_3, c_4) = f_1(x; c_1, c_2)/[1 + (x/c_3)^{c_2+c_4}] \quad \text{(ii)}$$

$$f_3(x; c_1, c_2, c_3, c_4, c_5, c_6) = f_1(x; c_1, c_2)/[1 + (x/c_3)^{c_2+c_4} + (x/c_5)^{c_2+c_6}] \quad \text{(iii)}$$

$$\sigma_0 = 1 \times 10^{-16}\ \text{cm}^2 \quad \text{(iv)}$$

$$E_\text{R} = 1.361 \times 10^{-2}\ \text{keV (Rydberg constant)} \quad \text{(v)}$$

$$E_1 = E - E_\text{th} \quad \text{(vi)}$$

$$E = \text{incident electron energy in keV} \quad \text{(vii)}$$

$$E_\text{th} = \text{threshold energy of reaction in keV.} \quad \text{(viii)}$$

The symbols x and c_i ($i = 1, 2, \ldots, 6$) in Eqs. (i)–(iii) denote dummy parameters. Depending on the formula to be chosen from the equations below, the value of E_1 or E_1/a_i ($i = 6$ or 8) is put into x; and a_1, a_2, etc. are put into c_i. The cross sections for the individual collisional processes are given by the following set of analytic expressions, according to the correlation between the "No." and "Eq." columns in Table I (read across two facing pages).

$$\sigma = f_2(E_1; a_1, a_2, a_3, a_4) \quad (1)$$

$$\sigma = f_1(E_1; a_1, a_2) + f_2(E_1; a_3, a_4, a_5, a_6) \quad (2)$$

$$\sigma = f_2(E_1; a_1, a_2, a_3, a_4) + a_5 f_2(E_1/a_6; a_1, a_2, a_3, a_4) + a_7 f_2(E_1/a_8; a_1, a_2, a_3, a_4) \quad (3)$$

$$\sigma = f_1(E_1; a_1, a_2) + f_2(E_1; a_3, a_4, a_5, a_6) + f_2(E_1; a_7, a_8, a_9, a_{10}) \quad (4)$$

$$\sigma = f_3(E_1; a_1, a_2, a_3, a_4, a_5, a_6) \quad (5)$$

$$\sigma = f_1(E_1; a_1, a_2) + f_3(E_1; a_3, a_4, a_5, a_6, a_7, a_8) \quad (6)$$

$$\sigma = f_2(E_1; a_1, a_2, a_3, a_4) + f_3(E_1; a_5, a_6, a_7, a_8, a_9, a_4) \quad (7)$$

$$\sigma = f_2(E_1; a_1, a_2, a_3, a_4) + f_3(E_1; a_5, a_6, a_7, a_8, a_9, a_{10}) \quad (8)$$

$$\sigma = f_1(E_1; a_1, a_2) + f_2(E_1; a_3, a_4, a_5, a_6) + f_3(E_1; a_7, a_8, a_9, a_{10}, a_{11}, a_{12}) \quad (9)$$

$$\sigma = \sigma_0 a_1 [\ln(E/E_\text{th}) + a_2]/[E_\text{th} E(1 + (a_3/E_1)^{a_4})]. \quad (10)$$

The use of such expressions allows one not only to interpolate but also to extrapolate the data to some extent, in contrast to polynomial fits, which frequently show physically unreasonable behavior just outside the energy range of the available data.

The number of adjustable parameters used in the analytic expressions is between 4 and 12 according to the type of function. The values of the adjustable parameters have been determined by least-squares fits to the data except for some values that were chosen to guarantee reasonable behavior outside the energy range of the available data. The values determined are given in the last six columns of Table I.

Cross sections obtained from the analytic expressions are compared with the experimental data in the set of graphs, which show that agreement is quite good. The root-mean-square and the maximum deviations of the expressions from the data are given in the fifth and sixth columns of Table I. An analogous example of use of Table I and the analytic expressions to calculate a cross section can be found in Ref. [86].

Acknowledgments

We are indebted to Professor Y. Itikawa of the Institute of Space and Astronautical Science for his invaluable comments and critical reading of the manuscript. We also express our thanks to Dr. M. Nakagawa and Dr. A. Hasegawa for their encouragement during this work.

References

1. I. Kanik, S. Trajmar, and J. C. Nickel, J. Geophys. Res. **98**, 7447 (1993) (Kanik et al. (1993a) in Graph legends)

2. W. Liu and G. A. Victor, Astrophys. J. **435**, 909 (1994)

3. G. García, C. Aragón, and J. Campos, Phys. Rev. A **42**, 4400 (1990)

4. I. Kanik, J. C. Nickel, and S. Trajmar, J. Phys. B **25**, 2189 (1992)

5. G. Karwasz, R. S. Brusa, A. Gasparoli, and A. Zecca, Chem. Phys. Lett. **211**, 529 (1993)

6. J. C. Gibson, L. A. Morgan, R. J. Gulley, M. J. Brunger, C. T. Bundschu, and S. J. Buckman, J. Phys. B **29**, 3197 (1996)

7. H. Tanaka, S. K. Srivastava, and A. Chutjian, J. Chem. Phys. **69**, 5329 (1978)

8. J. E. Land, J. Appl. Phys. **49**, 5716 (1979)

9. G. N. Haddad and H. B. Milloy, Aust. J. Phys. **36**, 473 (1983)

10. Y. Itikawa, ATOMIC DATA AND NUCLEAR DATA TABLES **21**, 69 (1978)

11. M. J. Mumma, E. J. Stone, and E. C. Zipf, J. Chem. Phys. **54**, 2627 (1971)

12. J. Zobel, U. Mayer, K. Junk, and H. Ehrhardt, J. Phys. B **29**, 813 (1996)

13. P. W. Zetner, I. Kanik, and S. Trajmar, J. Phys. B **31**, 2395 (1998)

14. W. C. Wells, W. L. Borst, and E. C. Zipf, Phys. Rev. A **8**, 2463 (1973); W. C. Wells and E. C. Zipf, J. Chem. Phys. **57**, 3583 (1972)

15. N. J. Manson and W. R. Newell, J. Phys. B **21**, 1293 (1988)

16. I. Kanik, M. Ratliff, and S. Trajmar, Chem. Phys. Lett. **208**, 341 (1993) (Kanik et al. (1993b) in Graph legends)

17. M. Ciocca, I. Kanik, and J. M. Ajello, Phys. Rev. A **55**, 3547 (1997)

18. L. R. LeClair, M. D. Brown, and J. W. McConkey, Chem. Phys. **189**, 769 (1994)

19. J. M. Furlong and W. R. Newell, J. Phys. B **29**, 331 (1996)

20. J. F. M. Aarts and F. J. de Heer, J. Chem. Phys. **52**, 5354 (1970) (Aarts and de Heer (1970a) in Graph legends)

21. E. N. Lassettre and S. M. Silverman, J. Chem. Phys. **40**, 1256 (1956); E. N. Lassettre and A. Skerbele, J. Chem. Phys. **54**, 1597 (1971)

22. I. Kanik, G. K. James, and J. M. Ajello, Phys. Rev. A **51**, 2067 (1995)

23. G. K. James, J. M. Ajello, I. Kanik, B. Franklin, and D. E. Shemansky, J. Phys. B **25**, 1481 (1992)

24. J. M. Ajello, J. Chem. Phys. **55**, 3158 (1971)

25. P. W. Erdman and E. C. Zipf, Planet. Space Sci. **31**, 317 (1983)

26. E. Hille and T. D. Märk, J. Chem. Phys. **69**, 4600 (1978)

27. R. S. Freund, R. C. Wetzel, and R. J. Shul, Phys. Rev. A **41**, 5861 (1990)

28. O. J. Orient and S. K. Srivastava, J. Chem. Phys. **78**, 2949 (1983)

29. C. Tian and C. R. Vidal, J. Phys. B **31**, 895 (1998) (Tian and Vidal (1998a) in Graph legends)

30. W. Hwang, Y.-K. Kim, and M. E. Rudd, J. Chem. Phys. **104**, 2956 (1996)

31. V. V. Skubenich, Opt. Spectrosk. **23**, 540 (1967)

32. J. F. M. Aarts and F. J. de Heer, Physica **49**, 425 (1970) (Aarts and de Heer (1970b) in Graph legends)

33. P. C. Cosby, J. Chem. Phys. **98**, 7804 (1993)

34. G. M. Lawrence, Phys. Rev. A **2**, 397 (1970)

35. K. R. Hoffman, M. S. Dababneh, Y.-F. Hsieh, W. E. Kauppila, V. Pol, J. H. Smart, and T. S. Stein, Phys. Rev. A **25**, 1393 (1982)

36. Ch. K. Kwan, Y.-F. Hsieh, W. E. Kauppila, S. J. Smith, T. S. Stein, and M. N. Uddin, Phys. Rev. A **27**, 1328 (1983)

37. O. Sueoka and S. Mori, J. Phys. Soc. Japan **53**, 2491 (1984)

38. C. Szmytkowski, A. Zecca, G. Karwasz, S. Oss, K. Maciąg, B. Marinković, R. S. Brusa, and R. Grisenti, J. Phys. B **20**, 5817 (1987)

39. G. Garcia and F. Manero, Phys. Rev. A **53**, 250 (1996)

40. D. F. Register, H. Nishimura, and S. Trajmar, J. Phys. B **13**, 1651 (1980)

41. I. Iga, J. C. Nogueria, and L. Mu-Tao, J. Phys. B **17**, L185 (1984)

42. I. Iga, M. G. P. Homem, K. T. Mazon, and M.-T. Lee, J. Phys. B **32**, 4373 (1999)

43. H. Tanaka, T. Ishikawa, T. Masai, T. Sagara, L. Boesten, M. Takekawa, Y. Itikawa, and M. Kimura, Phys. Rev. A **57**, 1798 (1998)

44. J. C. Gibson, M. A. Green, K. W. Trantham, S. J. Buckman, P. J. O. Teubner, and M. J. Brunger, J. Phys. B **32**, 213 (1999)

45. Y. Nakamura, Aust. J. Phys. **48**, 357 (1995)

46. T. D. Märk and E. Hille, J. Chem. Phys. **69**, 2492 (1978)

47. E. Krishnakumar, Int. J. Mass Spectrom. Ion Proc. **97**, 283 (1990)

48. H. C. Straub, B. G. Lindsay, K. A. Smith, and R. F. Stebbings, J. Chem. Phys. **105**, 4015 (1996)

49. C. Tian and C. R. Vidal, J. Chem. Phys. **108**, 927 (1998) (Tian and Vidal (1998b) in Graph legends)

50. C. Tian and C. R. Vidal, Phys. Rev. A **58**, 3783 (1998) (Tian and Vidal (1998c) in Graph legends)

51. J. W. McConkey, D. J. Burn, and J. M. Woolsey, J. Phys. B **1**, 71 (1968)

52. J. M. Ajello, J. Chem. Phys. **55**, 3169 (1971)

53. S. Tsurubuchi and T. Iwai, J. Phys. Soc. Jpn. **37**, 1077 (1974)

54. J. E. Mentall, M. A. Coplan, and R. J. Kushlis, J. Chem. Phys. **43**, 3867 (1973)

55. L. R. LeClair and J. W. McConkey, J. Phys. B **27**, 4039 (1994)

56. I. Kanik, J. M. Ajello, and G. K. James, Chem. Phys. Lett. **221**, 523 (1993) (Kanik et al. (1993c) in Graph legends)

57. E. Brüche, Ann. Phys. **1**, 93 (1929)

58. O. Sueoka, S. Mori, and Y. Katayama, J. Phys. B **19**, L373 (1986)

59. C. Szmytkowski, Chem. Phys. Lett. **136**, 363 (1987)

60. A. Zecca, G. Karwasz, S. Oss, R. Grisenti, and R. S. Brusa, J. Phys. B **20**, L133 (1987)

61. H. Nishimura and K. Yano, J. Phys. Soc. Jpn. **57**, 1951 (1988)

62. Z. Sağlam and N. Aktekin, J. Phys. B **24**, 3491 (1991)

63. A. Danjo and H. Nishimura, J. Phys. Soc. Jpn. **54**, 1224 (1985)

64. A. Katase, K. Ishibashi, Y. Matsumoto, T. Sakae, S. Maezono, E. Murakami, K. Watanabe, and H. Maki, J. Phys. B **19**, 2715 (1986)

65. T. W. Shyn and S. Y. Cho, Phys. Rev. A **36**, 5138 (1987)

66. W. M. Johnstone and W. R. Newell, J. Phys. B **24**, 3633 (1991)

67. T. W. Shyn and A. Grafe, Phys. Rev. A **46**, 4406 (1992)

68. M. Hayashi, "Atomic and Molecular Data for Radiotherapy," Report IAEA-TECDOC-506, p. 193, International Atomic Energy Agency (1989)

69. G. Seng and F. Linder, J. Phys. B **9**, 2539 (1976)

70. T. W. Shyn, S. Y. Cho, and T. E. Cravens, Phys. Rev. A **38**, 678 (1988)

71. J. Schutten, F. J. de Heer, H. R. Moustafa, A. J. H. Boerboom, and J. Kistemaker, J. Chem. Phys. **44**, 3924 (1966)

72. N. Lj. Djurić, I. M. Čadež, and M. V. Kurepa, Int. J. Mass Spectrom. Ion. Proc. **83**, R7 (1988)

73. H. C. Straub, B. G. Lindsay, K. A. Smith, and R. F. Stebbings, J. Chem. Phys. **108**, 109 (1998)

74. T. Ogawa, S. Ihara, N. Yonekura, T. Yasuda, and K. Nakashima, Chem. Phys. **168**, 145 (1992)

75. G. R. Möhlmann, K. H. Shima, and F. J. de Heer, Chem. Phys. **28**, 331 (1978)

76. M. J. Mumma and E. C. Zipf, J. Chem. Phys. **55**, 1661 (1971)

77. H. Tawara, Y. Itikawa, H. Nishimura, and M. Yoshino, J. Phys. Chem. Ref. Data **19**, 617 (1990)

78. G. R. Möhlmann and F. J. de Heer, Chem. Phys. **40**, 157 (1979)

79. C. I. M. Beenakker, F. J. de Heer, H. B. Krop, and G. R. Möhlmann, Chem. Phys. **6**, 445 (1974)

80. D. A. Vroom and F. J. de Heer, J. Chem. Phys. **50**, 1883 (1969)

81. U. Müller, Th. Bubel, and G. Schulz, Z. Phys. D **25**, 167 (1993)

82. I. V. Sushanin and S. M. Kishko, Opt. Spectros. **30**, 315 (1970)

83. H. D. Morgan and J. E. Mentall, J. Chem. Phys. **60**, 4734 (1974)

84. A. E. S. Green and R. J. McNeal, J. Geophys. Res. **76**, 133 (1971)

85. Y. Nakai, T. Shirai, T. Tabata, and R. Ito, ATOMIC DATA AND NUCLEAR DATA TABLES **37**, 69 (1987)

86. T. Tabata and T. Shirai, ATOMIC DATA AND NUCLEAR DATA TABLES **76**, 1 (2000)

87. W. Lotz, Z. Phys. **206**, 205 (1967)

Published online August 28, 2001

EXPLANATION OF TABLES

TABLE I. **Energy Ranges of Data, Fitting Errors, and Parameters of the Analytic Expressions for CO**

TABLE II. **Energy Ranges of Data, Fitting Errors, and Parameters of the Analytic Expressions for CO_2**

TABLE III. **Energy Ranges of Data, Fitting Errors, and Parameters of the Analytic Expressions for H_2O**

No.	Number label identifying a particular reaction process in the same sequence as in the Graphs.
Process	The relevant reaction process.
E_{min}	Minimum energy (in keV) of the recommended data.
E_{max}	Maximum energy (in keV) of the recommended data.
δ_{rms}	Root-mean-square relative deviation (in %) of the analytic expression from the data.
δ_{max}	Maximum relative deviation (in %) of the analytic expression from the data.
$E_{\delta_{max}}$	Energy (in keV) at which the relative deviation takes on the value δ_{max}.
Eq.	The identifying number of the equation to be used for deriving the recommended cross sections.
n	Number of applicable fit parameters.
E_{th}	Threshold energy of the reaction (in keV).
a_i $(i = 1, 2, \ldots, 12)$	Fit parameters.

The notation 1.23–1 means 1.23×10^{-1}.

EXPLANATION OF GRAPHS

GRAPHS. **Cross Section vs Electron Energy**

Graphs are numbered in the same sequence as in Tables I, II, and III.

Ordinate	Cross section in cm^2.
Abscissa	Electron energy in eV in the laboratory system.
Solid line	Recommended data from the analytic formula of the present work.
Symbols	Experimental data from sources as explained in the legends.

TABLE I. Energy Ranges of Data, Fitting Errors, and Parameters of the Analytic Expressions for CO

See page 153 for Explanation of Tables

No.	Process	E_{min}	E_{max}	δ_{rms}	δ_{max}	$E_{\delta_{max}}$
1	Total Scattering	1.00−3	5.25	2.4	1.1+1	2.00−3
2	Elastic Scattering	1.00−3	1.00	8.8	3.4+1	1.00−1
3	Momentum transfer	1.00−3	1.00−1	1.1+1	2.7+1	3.00−2
4	Vibrational Excitation for $v = 0 \rightarrow 1$	1.00−3	3.00−2	9.8	1.8+1	1.25−3
5	Total Electronic Excitation	6.10−3	1.00	5.1	1.2+1	9.00−1
6	Excitation to CO($A\ ^1\Pi; v = 0$)	1.25−2	3.50−1	2.4	4.9	2.00−1
7	Excitation to CO($A\ ^1\Pi; v = 1$)	1.25−2	3.50−1	0.7	1.8	3.00−1
8	Excitation to CO($A\ ^1\Pi; v = 2$)	1.25−2	3.50−1	1.7	3.4	6.25−2
9	Excitation to CO($A\ ^1\Pi; v = 3$)	1.25−2	3.50−1	3.4	9.8	1.50−1
10	Excitation to CO($A\ ^1\Pi; v = 4$)	1.25−2	3.50−1	3.5	1.2+1	1.50−1
11	Excitation to CO($I\ ^1\Sigma^-$)	1.00−2	4.50−2	2.5	5.8	1.75−2
12	Excitation to CO($B\ ^1\Sigma^+$)	1.00−1	1.00−1	0.0	0.0	1.00−1
13	Excitation to CO($C\ ^1\Sigma^+$)	1.00−1	1.00−1	0.0	0.0	1.00−1
14	Excitation to CO($E\ ^1\Pi$)	5.00−2	5.00−1	0.4	0.8	7.50−2
15	Excitation to CO($a\ ^3\Pi$)	7.00−3	5.00−2	2.4	4.7	8.00−3
16	Emission from CO($A\ ^1\Pi$–$X\ ^1\Sigma^+; v = 0$–1) at 1597 Å	1.30−2	5.00	5.3	1.6+1	3.50−1
17	Emission from CO($B\ ^1\Sigma^+$–$X\ ^1\Sigma^+; v = 0$–0) at 1150 Å	2.00−2	5.00	1.2+1	4.4+1	1.00−1
18	Emission from CO($C\ ^1\Sigma^+$–$X\ ^1\Sigma^+; v = 0$–0) at 1088 Å	2.00−2	2.00	2.2	3.6	1.00
19	Emission from CO($E\ ^1\Pi^+$–$X\ ^1\Sigma^+; v = 0$–0) at 1076 Å	5.00−2	5.00−1	2.5	7.2	3.50−1
20	Emission from CO($A\ ^1\Pi$–$X\ ^1\Sigma^+; v =$ total) at 1270–2000 Å	9.00−3	3.00−1	0.8	1.8	2.50−2
21	Emission from CO($a\ ^3\Pi$–$X\ ^1\Sigma^+; v = 1$–4) at 2389 Å	6.50−3	3.00−1	5.2	1.0+1	1.00−1
22	Total Ionization	1.75−2	6.00−1	2.0	4.8	2.50−2
23	CO^+ Production	1.75−2	6.00−1	1.3	3.2	3.50−2
24	C^+ Production	2.50−2	6.00−1	5.9	2.1+1	3.00−2
25	O^+ Production	3.00−2	6.00−1	3.9	1.0+1	5.00−2
26	CO^{2+} Production	5.00−2	6.00−1	5.8	1.2+1	7.00−2

TABLE I. Energy Ranges of Data, Fitting Errors, and Parameters of the Analytic Expressions for CO

See page 153 for Explanation of Tables

No.	Eq.	n	E_{th}	a_1 a_7	a_2 a_8	a_3 a_9	a_4 a_{10}	a_5 a_{11}	a_6 a_{12}
1	3	8	0.00	2.190+4 5.300−2	3.190 7.930−1	2.084−3	3.880	1.722+1	2.210−1
2	3	8	0.00	1.800+4 3.620−3	3.190 5.720−1	2.100−3	4.900	5.670+1	5.500−1
3	8	10	0.00	3.350+3 7.500−3	2.300 1.087	1.890−3 2.900−1	7.500 3.400	2.440+1	2.180−1
4	3	8	2.70−4	9.130+4 1.980−2	4.440 1.000+1	1.740−3 .	4.630	7.660−1	2.680
5	7	9	6.00−3	2.810 2.050−2	3.610−1 8.400−1	1.620−3 1.050−1	2.580	5.530	1.110
6	1	4	7.80−3	1.740−1	1.100	9.110−3	4.600−1		
7	1	4	7.20−3	3.020−1	1.011	1.009−2	4.749−1		
8	1	4	7.90−3	2.920−1	9.520−1	1.194−2	5.160−1		
9	1	4	8.60−3	2.650−1	1.040	8.500−3	4.380−1		
10	1	4	8.70−3	1.350−1	8.040−1	1.220−2	4.970−1		
11	3	8	8.10−3	2.600 1.000−1	4.280 5.000−1	5.390−3	1.030	1.190−3	1.190
12	1	4	1.08−2	9.580−2	4.700−1	2.500−2	8.030−1		
13	1	4	1.14−2	6.579−2	8.770−1	6.270−2	7.490−1		
14	10	4	1.15−2	1.407−5	8.100	1.520−1	1.096		
15	3	8	6.04−3	3.690+1 8.440−3	1.790 2.160−1	3.260−3	1.570	4.060+1	1.000+1
16	1	4	7.80−3	2.280−2	1.820−1	6.300−2	8.750−1		
17	1	4	1.08−2	5.350−2	4.700−1	2.500−2	8.030−1		
18	1	4	1.14−2	3.881−2	8.770−1	6.270−2	7.490−1		
19	10	4	1.15−2	1.509−6	8.100	1.520−1	1.096		
20	5	6	8.00−3	1.751+2	2.666	1.236−3	−3.477−1	2.854−3	5.428−1
21	3	8	6.00−3	1.360+2 5.030−4	2.890 9.410−2	3.240−3	1.140	6.930+4	3.760
22	10	4	1.41−2	2.726−3	2.800−2	5.300−2	1.058		
23	5	6	1.40−2	1.825	1.829	1.390−2	−1.390−1	4.380−2	9.940−1
24	1	4	2.24−2	1.216−1	9.360−1	8.530−2	8.720−1		
25	5	6	2.47−2	2.100−1	4.080	7.080−3	−1.560	2.100−2	7.390−1
26	1	4	4.18−2	1.868−3	1.502	5.890−2	7.480−1		

TABLE I. Energy Ranges of Data, Fitting Errors, and Parameters of the Analytic Expressions for CO

See page 153 for Explanation of Tables

No.	Process	E_{min}	E_{max}	δ_{rms}	δ_{max}	$E_{\delta_{max}}$
27	O^{2+} Production	8.00−2	6.00−1	9.6	2.5+1	3.00−1
28	C^{2+} Production	6.00−2	6.00−1	6.2	1.9+1	7.00−2
29	Excitation to $CO^+(X\ ^2\Sigma^+)$	5.00−2	1.00	5.1	1.1+1	6.00−1
30	Excitation to $CO^+(A\ ^2\Pi)$	1.75−2	5.00	6.2	1.8+1	5.00−2
31	Excitation to $CO^+(B\ ^2\Sigma^+)$	2.25−2	5.00	3.7	1.3+1	1.50−1
32	Emission from $CO^+(A\ ^2\Pi–X\ ^2\Sigma^+; v = 3–0)$ at 4011 Å	2.00−2	5.00	6.1	1.7+1	3.00−1
33	Emission from $CO^+(B\ ^2\Sigma^+–X\ ^2\Sigma^+; v = 0–0)$ at 2190 Å	5.00−2	5.00	1.2	2.1	2.00−1
34	Emission from $CO^+(A\ ^2\Pi–X\ ^2\Sigma^+; v =$ total) at 3000–6500 Å	2.20−2	3.00−1	0.4	0.8	4.00−2
35	Emission from $CO^+(B\ ^2\Sigma^+–X\ ^2\Sigma^+; v =$ total) at 1800–3200 Å	2.00−2	3.00−1	3.0	9.6	2.50−2
36	$C(^3P) + O(^3P)$ Production	1.35−2	1.99−1	6.9	1.4+1	1.85−2
37	$O(^1S)$ Production	1.80−2	5.00−1	2.2	4.5	3.00−2
38	Emission from C I$(2p3d\ ^3D^o, ^3F^o, 2p4s\ ^3P^o–2p^2\ ^3P)$ at 1278−1280 Å	2.50−2	2.00	5.4	1.9+1	1.00−1
39	Emission from O I$(2p^33s\ ^3S^o–2p^4\ ^3P)$ at 1304 Å	2.50−2	4.00	7.5	2.3+1	2.50−2
40	Emission from C II$(2s2p^2\ ^2D–2s^22p\ ^2P^o)$ at 1335 Å	4.00−2	5.00	9.3	2.1+1	3.00−1
41	Emission from O I$(2p^33p\ ^3P–2p^33s\ ^3S^o)$ at 8447 Å	4.90−2	7.71−1	0.5	1.5	5.10−2

TABLE I. Energy Ranges of Data, Fitting Errors, and Parameters of the Analytic Expressions for CO

See page 153 for Explanation of Tables

No.	Eq.	n	E_{th}	a_1 a_7	a_2 a_8	a_3 a_9	a_4 a_{10}	a_5 a_{11}	a_6 a_{12}
27	1	4	5.98−2	1.040−4	1.970	1.050−1	7.100−1		
28	1	4	4.68−2	3.790−4	2.108	9.300−2	6.370−1		
29	1	4	1.40−2	5.760−1	7.100−1	5.600−2	8.380−1		
30	5	6	1.66−2	1.880+6	6.160	6.940−4	−9.430−1	2.260−3	7.060−1
31	5	6	1.97−2	1.550−1	9.840−1	5.100−2	1.700−1	1.260−1	9.500−1
32	5	6	1.71−2	8.170−1	2.580	4.270−3	−4.820−1	1.630−2	7.700−1
33	5	6	1.97−2	6.310−2	6.460−1	1.250−1	6.030−1	3.530−1	1.050
34	5	6	1.65−2	1.980	2.221	7.400−3	−2.240−1	5.900−2	2.310
35	1	4	1.97−2	1.988−1	6.610−1	1.280−1	6.970−1		
36	1	4	1.11−2	7.040−1	1.084	2.680−2	5.700−1		
37	1	4	1.53−2	1.627−3	1.070	7.440−2	6.980−1		
38	1	4	2.08−2	4.100−3	6.910−1	8.560−2	8.590−1		
39	1	4	2.06−2	2.032−3	1.270	6.960−2	8.130−1		
40	1	4	3.16−2	1.900−2	9.190−1	7.900−2	8.540−1		
41	5	6	1.26−2	1.246−4	4.260	3.680−2	−5.300−1	4.400−2	7.510−1

TABLE II. Energy Ranges of Data, Fitting Errors, and Parameters of the Analytic Expressions for CO_2

See page 153 for Explanation of Tables

No.	Process	E_{min}	E_{max}	δ_{rms}	δ_{max}	$E_{\delta_{max}}$
42	Total Scattering	5.00−4	5.00	5.8	3.1+1	4.00−3
43	Elastic Scattering	1.00−3	1.00	1.3+1	2.8+1	4.00−2
44	Momentum Transfer	1.50−3	1.00	1.1+1	1.9+1	2.00−2
45	Total Ionization	1.50−2	1.00	7.5	4.5+1	1.50−2
46	CO_2^+ Production	1.50−2	1.00	5.2	3.1+1	2.00−2
47	CO^+ Production	2.50−2	1.00	7.3	2.3+1	2.50−2
48	$CO^+ + O$ Production	2.50−2	5.95−1	1.2	3.1	5.50−2
49	O^+ Production	2.50−2	1.00	4.2	1.8+1	2.50−2
50	$O^+ + C + O$ Production	2.50−2	5.95−1	4.5	1.2+1	2.50−2
51	C^+ Production	3.00−2	1.00	7.5	4.7+1	3.00−2
52	$C^+ + O + O$ Production	3.50−2	5.95−1	2.2	7.1	4.00−2
53	CO_2^{2+} Production	4.50−2	1.00	7.5	2.9+1	4.50−2
54	$O^+ + CO^+$ Production	4.50−2	5.95−1	1.0	2.8	4.95−1
55	$2O^+ + C$ Production	4.50−2	5.95−1	1.8+1	6.9+1	4.50−2
56	$C^+ + O^+ + O$ Production	4.50−2	5.95−1	6.6	2.2+1	5.50−2
57	O^{2+} Production	8.00−2	1.00	2.0+1	5.7+1	1.00−1
58	C^{2+} Production	8.00−2	1.00	1.2+1	3.0+1	8.00−2
59	Emission from $CO_2^+(A\ ^2\Pi_u – X\ ^2\Pi_g; v = \text{total})$ at 2930–4390 Å	2.00−2	2.00	8.1	2.0+1	3.00−2
60	Emission from $CO_2^+(B\ ^2\Sigma_u^+ – X\ ^2\Pi_g; v = \text{total})$ at 2880–2900 Å	2.00−2	2.00	6.5	1.7+1	2.00−2
61	Dissociative Excitation to $CO(A\ ^1\Pi; v = 0/1/2)$	1.50−2	3.50−1	5.6	1.3+1	2.00−2
62	Dissociative Excitation to $CO(A\ ^1\Pi; v = 3/4)$	1.50−2	3.50−1	3.4	7.7	3.50−1
63	Emission from $CO(A\ ^1\Pi – X\ ^1\Sigma^+; v = \text{total})$ at 1350–1730 Å	3.00−2	3.00−1	0.5	0.8	1.60−1
64	Emission from $CO(a\ ^3\Pi – X\ ^1\Sigma^+; v = 0–1)$ at 2158 Å	1.30−2	3.00−1	0.7	1.3	4.00−2
65	Emission from $CO^+(B\ ^2\Sigma^+ – X\ ^2\Sigma^+; v = \text{total})$ at 2040–2510 Å	2.70−2	3.00−1	0.6	1.2	2.50−1
66	$O(^1S)$ Production	1.20−2	1.00	1.9	6.4	1.40−2
67	Emission from C I$(2p3d\ ^3D^o, ^3F^o, 2p4s\ ^3P^o – 2p^2\ ^3P)$ at 1278−1280 Å	2.80−2	3.00−1	0.6	1.1	4.00−2
68	Emission from O I$(2p^3 3s\ ^3S^o – 2p^4\ ^3P)$ at 1304 Å	2.30−2	3.00−1	1.4	2.7	2.50−2
69	Emission from C II$(2s2p^2\ ^2D – 2s^2 2p\ ^2P^o)$ at 1335 Å	4.50−2	3.00−1	2.5	4.5	5.00−2

TABLE II. Energy Ranges of Data, Fitting Errors, and Parameters of the Analytic Expressions for CO_2

See page 153 for Explanation of Tables

No.	Eq.	n	E_{th}	a_1	a_2	a_3	a_4	a_5	a_6
				a_7	a_8	a_9	a_{10}	a_{11}	a_{12}
42	9	12	0.00	5.820−1	−9.950−1	8.870+4	6.760	3.882−3	1.030+1
				2.990+1	1.490	1.310−2	2.200−1	3.300−2	9.300−1
43	4	10	0.00	7.360−1	−7.300−1	2.140+5	8.200	3.810−3	1.000+1
				2.480+1	1.790	1.334−2	5.800−1		
44	4	10	0.00	1.680−1	−1.183	8.190+1	2.700	4.250−3	2.000+1
				1.450+1	1.090	1.910−2	1.288		
45	10	4	1.38−2	4.010−3	6.900−1	9.700−2	1.193		
46	10	4	1.38−2	2.990−3	3.600−1	1.010−1	9.040−1		
47	5	6	1.95−2	8.300−1	3.310	9.500−3	−4.600−1	2.210−2	9.600−1
48	5	6	1.95−2	4.830−1	3.062	1.266−2	−7.500−2	2.840−2	1.083
49	1	4	1.90−2	1.367−1	1.171	1.024−1	8.460−1		
50	5	6	1.91−2	1.640−1	1.081	8.300−2	7.300−1	1.800−1	7.300−1
51	5	6	2.78−2	1.850−1	2.200	1.290−2	−6.500−1	3.960−2	9.300−1
52	5	6	2.78−2	9.560−2	1.563	3.640−2	5.220−1	2.100−1	2.600
53	10	4	3.72−2	4.490−6	6.000+1	7.930−2	1.873		
54	5	6	3.31−2	2.198−2	2.427	2.870−2	−2.800−1	6.140−2	1.160
55	1	4	4.38−2	8.990−3	8.760−1	1.890−1	1.330		
56	1	4	4.14−2	9.460−3	1.483	1.160−1	9.760−1		
57	1	4	5.42−2	1.400−5	2.520	1.460−1	9.000−1		
58	1	4	5.22−2	4.830−5	2.040	1.360−1	8.380−1		
59	5	6	1.73−2	2.380−1	9.470−1	9.600−2	6.000−1	8.500−1	2.800
60	5	6	1.81−2	2.950−1	1.300	1.400−2	−4.900−1	5.900−2	7.800−1
61	1	4	1.36−2	1.140−2	5.700−1	1.280−2	3.730−1		
62	1	4	1.41−2	2.650−3	4.030−1	4.080−2	6.250−1		
63	1	4	1.35−2	1.282−2	−4.700−3	4.190−1	1.720		
64	5	6	1.15−2	2.789+1	2.601	4.450−3	−3.188−1	1.203−2	5.857−1
65	5	6	2.51−2	8.268−2	1.334	2.583−3	−2.549−1	4.560−2	1.658
66	5	6	1.10−2	3.160−1	1.046	1.210−2	1.320−1	5.140−2	9.300−1
67	5	6	2.62−2	5.072−1	2.694	1.599−3	−3.730−1	1.006−2	1.141
68	1	4	2.10−2	3.990−3	8.480−1	6.350−2	6.550−1		
69	1	4	4.30−2	4.310−3	7.070−1	8.960−2	6.720−1		

TABLE III. Energy Ranges of Data, Fitting Errors, and Parameters of the Analytic Expressions for H_2O

See page 153 for Explanation of Tables

No.	Process	E_{min}	E_{max}	δ_{rms}	δ_{max}	$E_{\delta_{max}}$
70	Total Scattering	1.00−3	3.00	4.9	1.8+1	7.00−3
71	Elastic Scattering	2.20−3	1.00	1.2+1	4.0+1	1.00−1
72	Momentum Transfer	2.20−3	1.00	1.3+1	4.4+1	5.00−2
73	Vibrational Excitation (Bending)	3.50−4	2.00−2	6.5	1.7+1	8.00−4
74	Vibrational Excitation (Stretching)	6.40−4	2.00−2	1.0+1	2.0+1	7.80−4
75	Total Ionization	1.35−2	1.00	5.3	2.0+1	1.35−2
76	H_2O^+ Production	2.00−2	2.00	2.1	3.9	1.00
77	OH^+ Production	2.00−2	2.00	2.4	4.7	1.00−1
78	O^+ Production	2.00−2	2.00	1.8+1	3.8+1	3.00−2
79	O^{2+} Production	9.00−2	1.00	9.4	2.5+1	1.10−1
80	H_2^+ Production	3.00−2	1.00	7.4	2.6+1	7.00−1
81	H^+ Production	2.00−2	1.00	3.7	1.1+1	2.25−2
82	H($n = 3$) Production	5.00−2	1.50	0.7	1.1	7.00−1
83	H($n = 4$) Production	5.00−2	1.00	0.9	1.5	3.00−1
84	Lyman-α Emission	2.00−2	2.00	3.7	1.3+1	3.00−2
85	Balmer-α Emission	2.00−2	2.00	2.2	6.4	5.00−2
86	Balmer-β Emission	4.00−2	1.00	1.6	4.9	5.00−2
87	Balmer-γ Emission	5.00−2	6.00	1.2	2.5	3.00−1
88	Balmer-δ Emission	5.00−2	6.00	1.8	4.1	6.00
89	Emission from OH($A\ ^2\Sigma^+ – X\ ^2\Pi; \delta v = 0$) at 3064 Å	1.10−2	1.00	3.2	9.5	4.00−2
90	Emission from O I($2p^3 3s\ ^3S^o – 2p^4\ ^3P$) at 1304 Å	2.73−2	2.80−1	1.9	3.5	5.00−2
91	Emission from O I($2p^3 3p\ ^5P – 2p^3 3s\ ^5S^o$) at 7774 Å	4.01−2	1.00	4.8	1.4+1	7.00−1
92	Emission from O I($2p^3 3p\ ^3P – 2p^3 3s\ ^3S^o$) at 8447 Å	4.01−2	1.00	1.7	5.0	1.40−1

TABLE III. Energy Ranges of Data, Fitting Errors, and Parameters of the Analytic Expressions for H_2O

See page 153 for Explanation of Tables

No.	Eq.	n	E_{th}	a_1	a_2	a_3	a_4	a_5	a_6
				a_7	a_8	a_9	a_{10}	a_{11}	a_{12}
70	6	8	0.00	3.420	−9.170−1	1.400+2	2.200	5.650−3	3.350−1
				1.850−2	1.210				
71	2	6	0.00	6.730−1	−1.200	3.700+1	9.700−1	1.080−2	8.810−1
72	2	6	0.00	6.340−1	−1.197	2.360+1	1.570	1.168−2	1.313
73	3	8	2.00−4	1.820+2	−1.400−2	1.500−6	1.020	2.510−1	8.400−1
				1.310−2	1.800				
74	3	8	4.50−4	2.060+2	−9.940−1	4.260−7	2.380	7.710−1	4.750−1
				1.070−2	3.430				
75	10	4	1.26−2	2.161−3	3.490−1	7.430−2	1.109		
76	5	6	1.26−2	1.180+2	4.960	4.120−3	−6.720−1	9.020−3	7.730−1
77	5	6	1.80−2	1.562−1	8.570−1	8.700−2	4.560−1	1.510−1	1.000
78	1	4	1.86−2	6.190−3	1.028	1.360−1	8.990−1		
79	1	4	5.37−2	3.540−6	3.300	1.078−1	7.550−1		
80	5	6	2.04−2	1.310−3	3.650	1.450−2	−1.370−1	3.180−2	1.080
81	1	4	1.87−2	6.397−2	1.390	8.240−2	7.690−1		
82	1	4	6.63−3	7.700−3	1.621	7.390−2	8.511−1		
83	1	4	5.97−3	1.556−3	1.773	7.010−2	8.170−1		
84	1	4	1.53−2	3.716−2	1.057	8.130−2	8.650−1		
85	1	4	1.72−2	1.113−2	1.074	7.490−2	8.680−1		
86	1	4	1.79−2	1.853−3	1.201	6.700−2	8.270−1		
87	1	4	1.82−2	2.474−3	3.820−1	9.740−2	9.171−1		
88	1	4	1.83−2	8.231−4	4.260−1	8.260−2	9.039−1		
89	5	6	9.10−3	2.950+1	3.360	2.210−3	−8.600−2	4.920−3	8.030−1
90	1	4	1.91−2	5.362−4	1.394	7.780−2	9.710−1		
91	1	4	1.57−2	5.880−4	1.065	5.670−2	1.048		
92	1	4	1.59−2	8.360−4	1.040	8.650−2	9.670−1		

GRAPHS. Cross Section vs Electron Energy

See page 153 for Explanation of Graphs

GRAPH 1

Total Scattering/C0

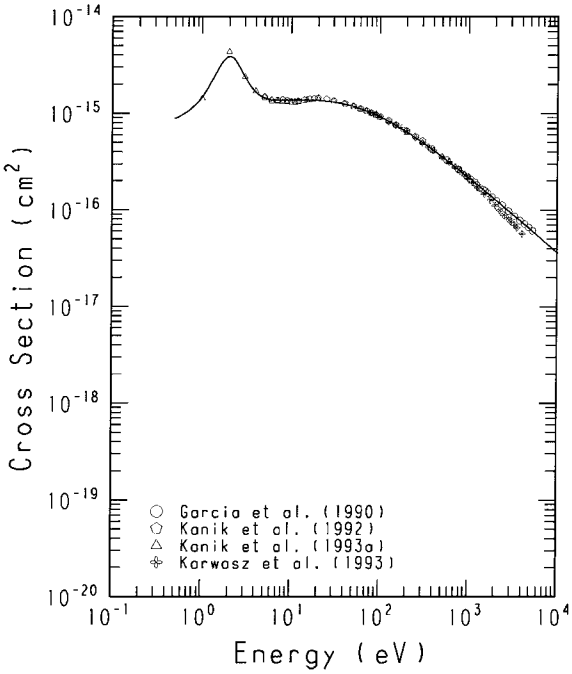

GRAPH 3

Momentum Transfer/C0

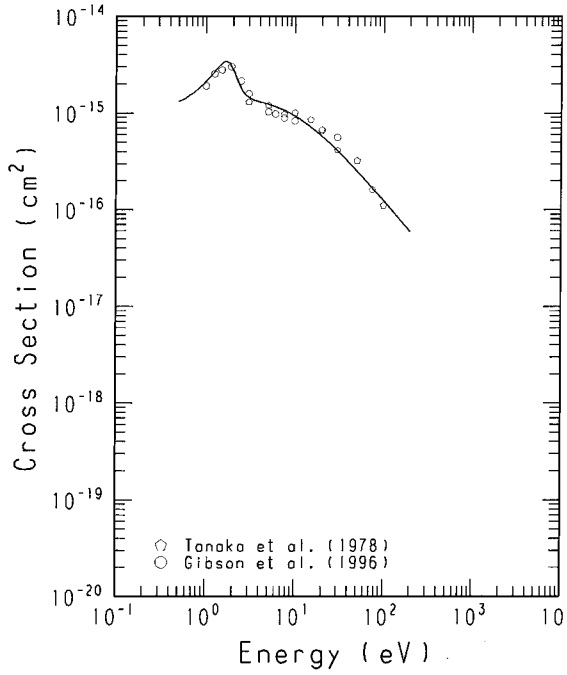

GRAPH 2

Elastic Scattering/C0

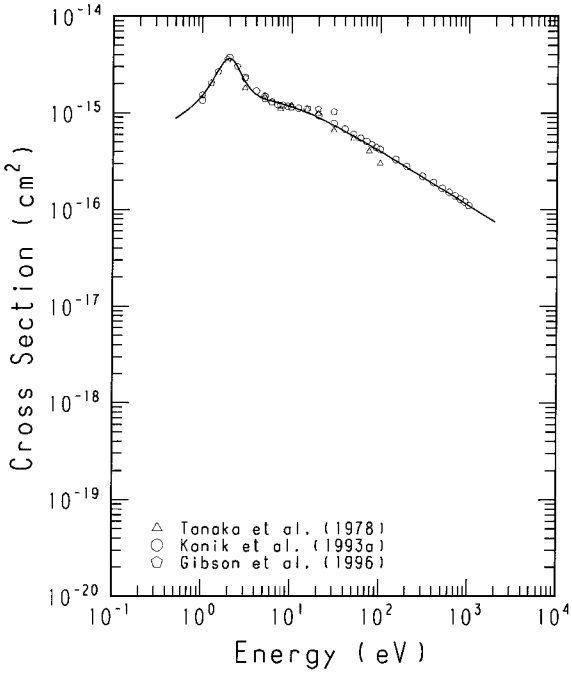

GRAPH 4

Vib. Exc. for v=0 → 1/C0

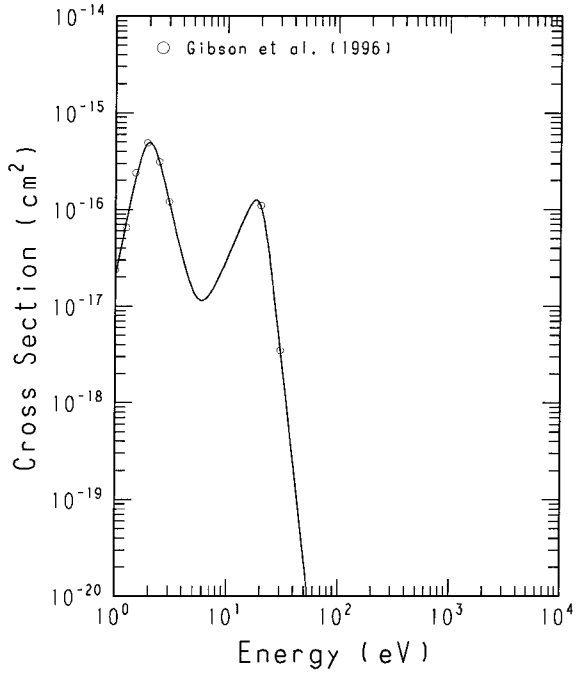

GRAPHS. Cross Section vs Electron Energy

See page 153 for Explanation of Graphs

GRAPH 5

Total Elec. Exc./CO

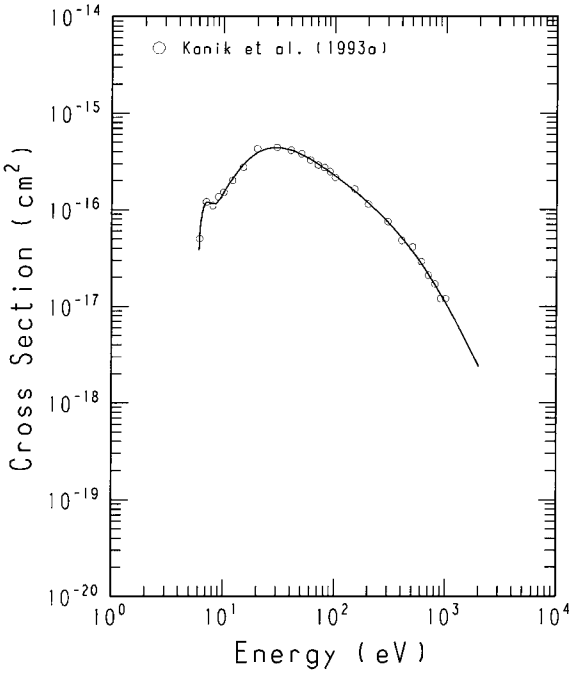

GRAPH 7

Exc. to (A $^1\Pi$; v=1)/CO

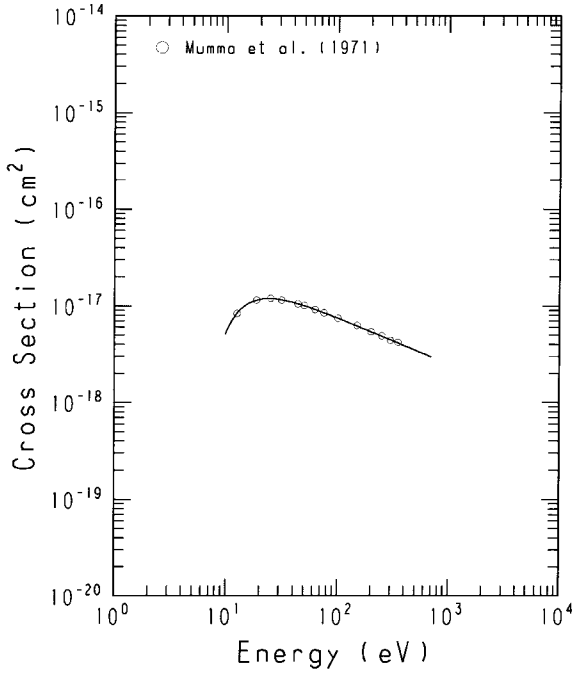

GRAPH 6

Exc. to (A $^1\Pi$; v=0)/CO

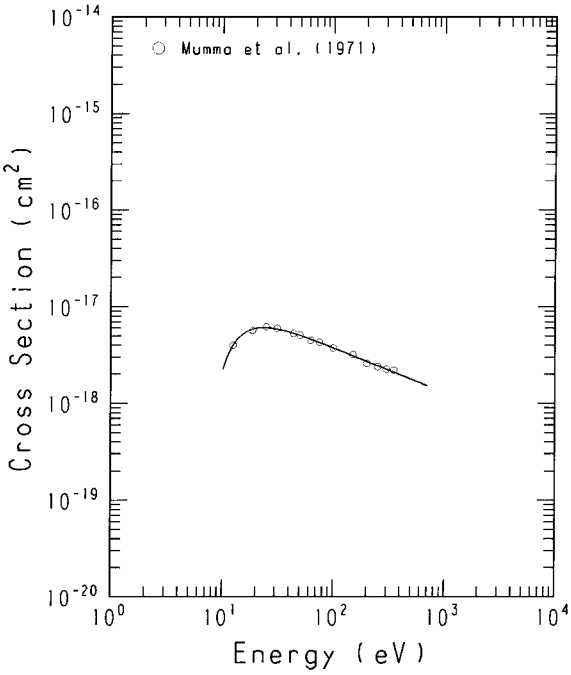

GRAPH 8

Exc. to (A $^1\Pi$; v=2)/CO

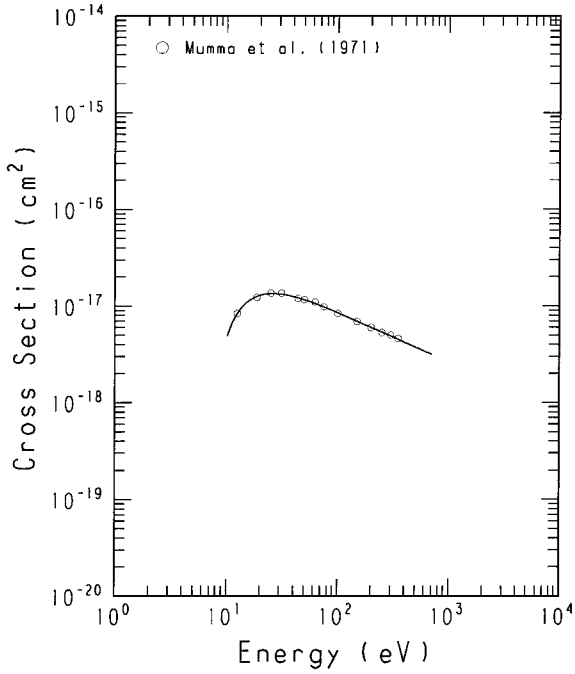

GRAPHS. Cross Section vs Electron Energy

See page 153 for Explanation of Graphs

GRAPH 9

Exc. to (A $^1\Pi$; v=3)/CO

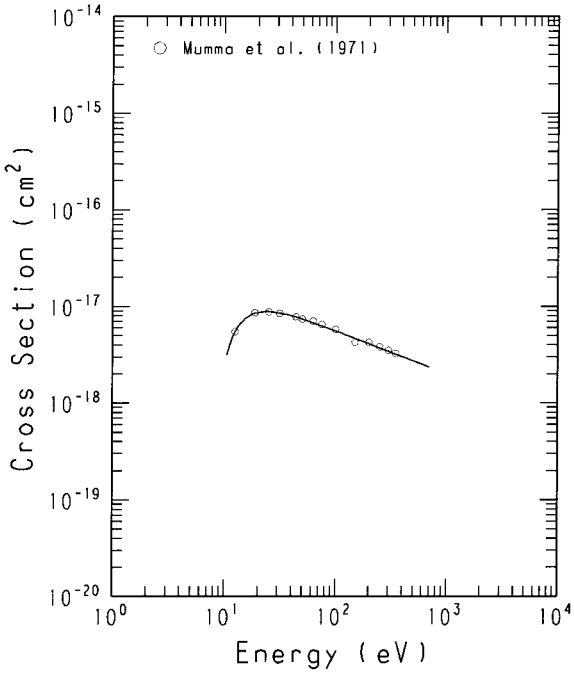

GRAPH 11

Exc. to (I $^1\Sigma^-$)/CO

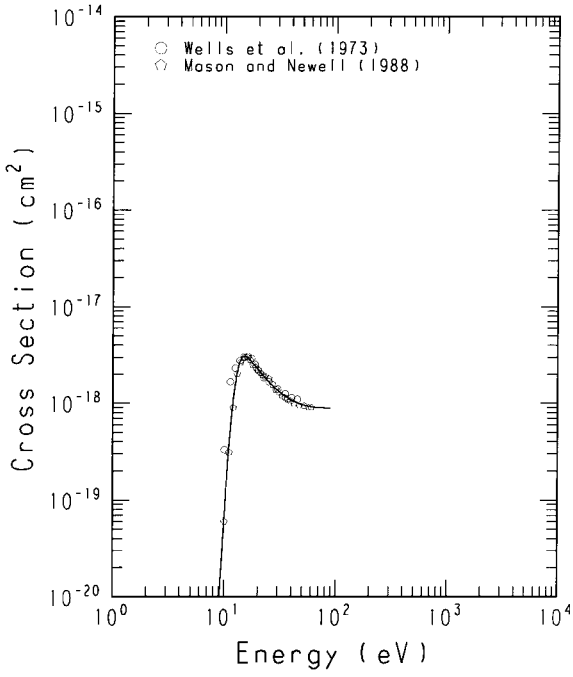

GRAPH 10

Exc. to (A $^1\Pi$; v=4)/CO

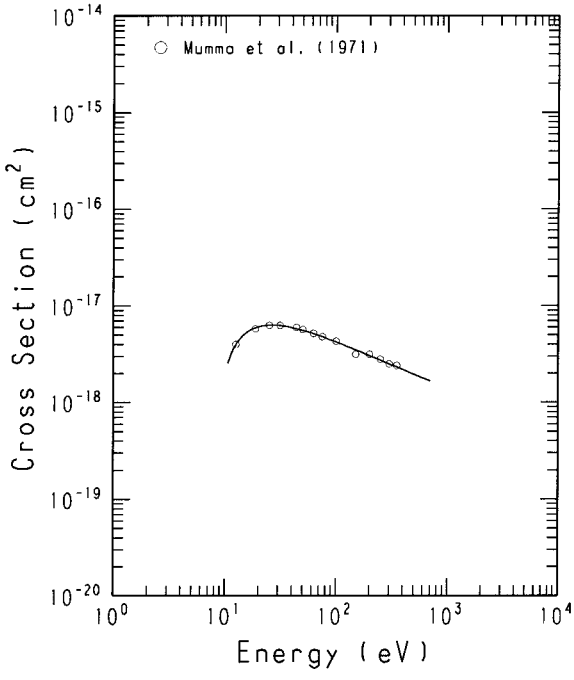

GRAPH 12

Exc. to (B $^1\Sigma^+$)/CO

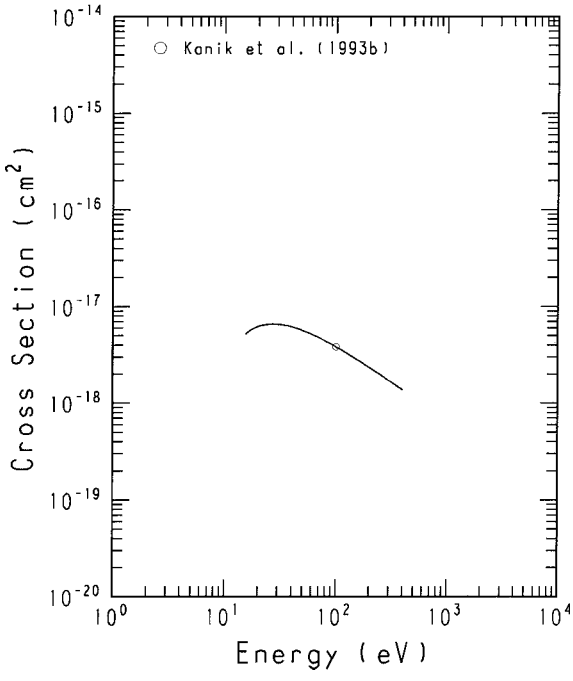

GRAPHS. Cross Section vs Electron Energy

See page 153 for Explanation of Graphs

GRAPH 13

Exc. to (C $^1\Sigma^+$)/C0

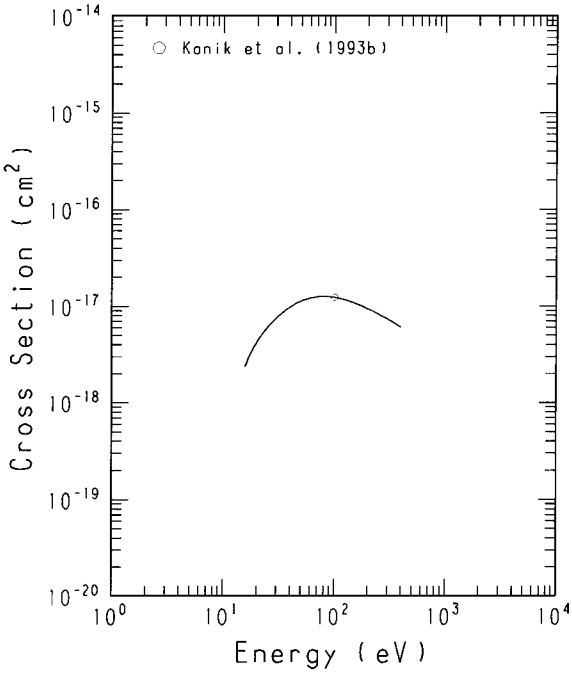

GRAPH 15

Exc. to (a $^3\Pi$)/C0

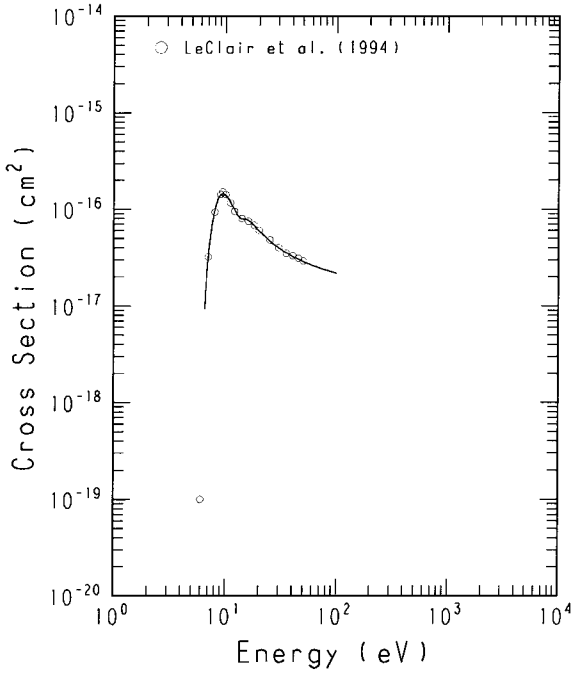

GRAPH 14

Exc. to (E $^1\Pi$)/C0

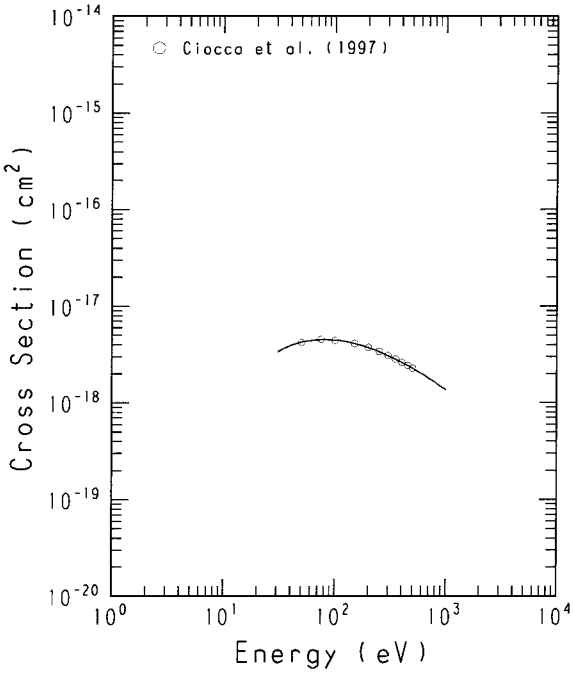

GRAPH 16

(A $^1\Pi$-X $^1\Sigma^+$; v=0-1)/C0 at 1597A

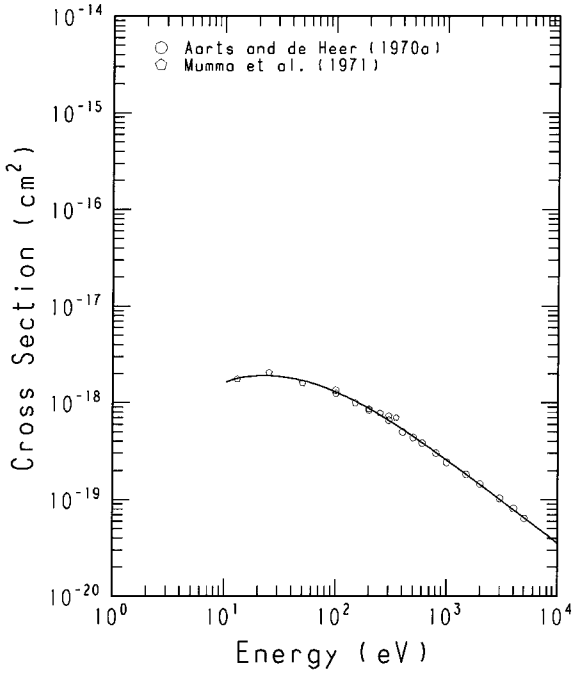

GRAPHS. Cross Section vs Electron Energy

See page 153 for Explanation of Graphs

GRAPH 17

(B $^1\Sigma^+$-X $^1\Sigma^+$;v=0-0)/CO at 1150A

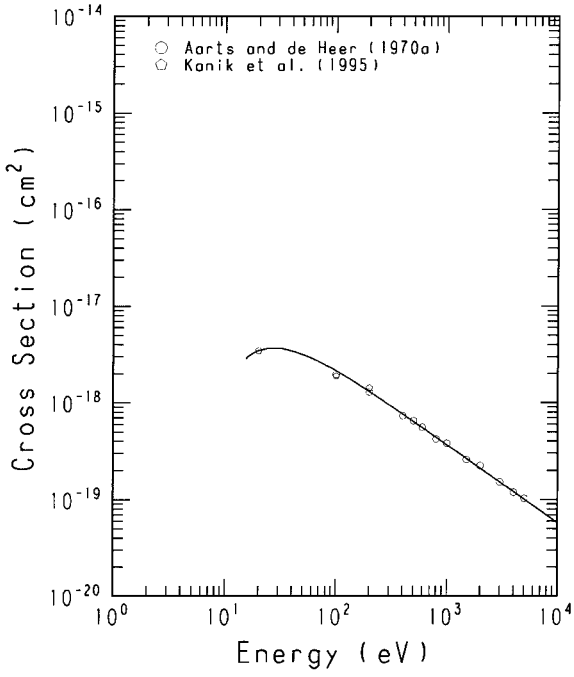

GRAPH 18

(C $^1\Sigma^+$-X $^1\Sigma^+$;v=0-0)/CO at 1088A

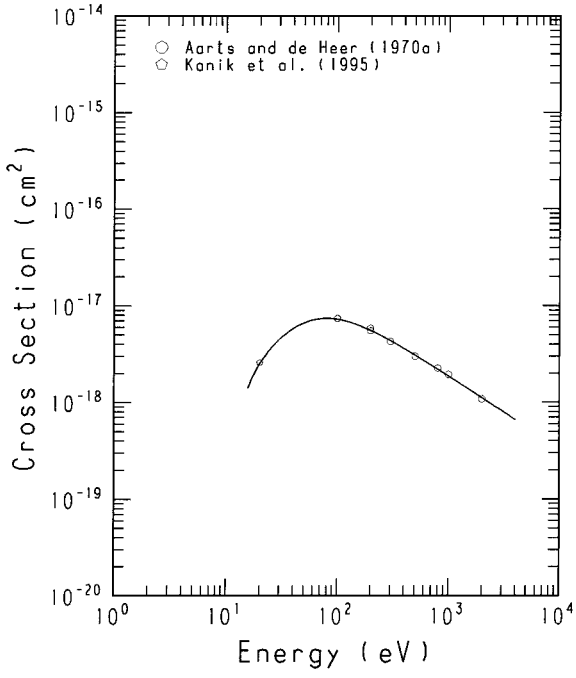

GRAPH 19

(E $^1\Pi^+$-X $^1\Sigma^+$;v=0-0)/CO at 1076A

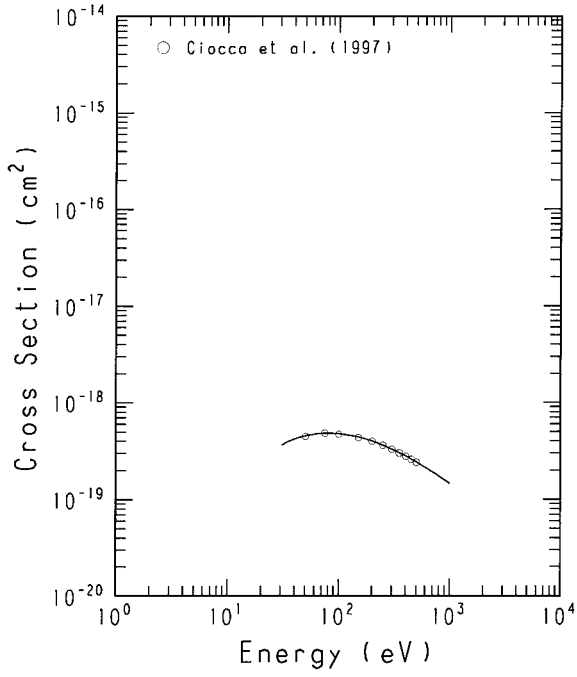

GRAPH 20

(A $^1\Pi$-X $^1\Sigma^+$;v=total)/CO at 1270-2000A

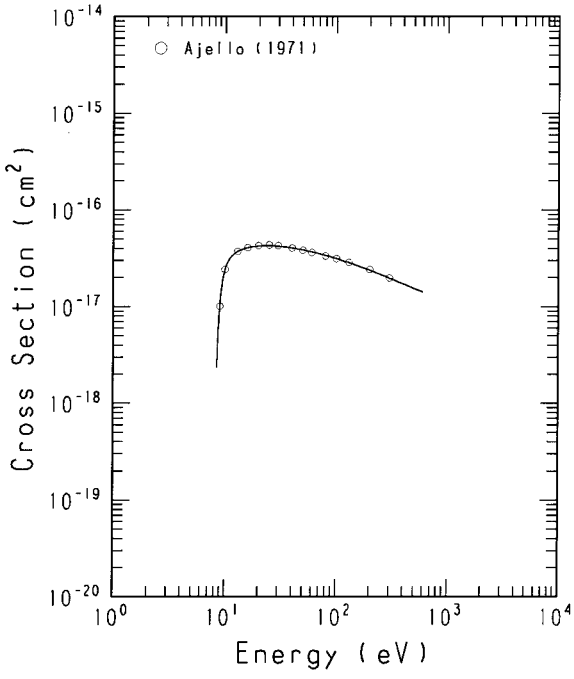

GRAPHS. Cross Section vs Electron Energy

See page 153 for Explanation of Graphs

GRAPH 21

(a $^3\Pi$-X $^1\Sigma^+$; v=1-4)/CO at 2389A

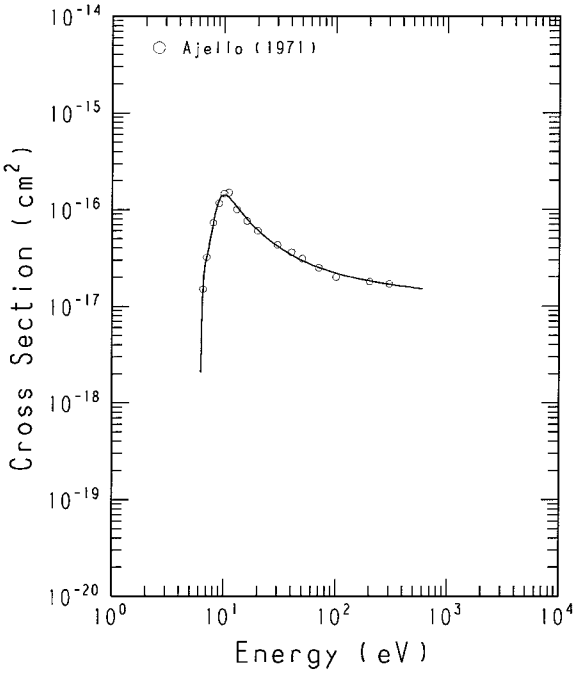

GRAPH 22

Total Ionization/CO

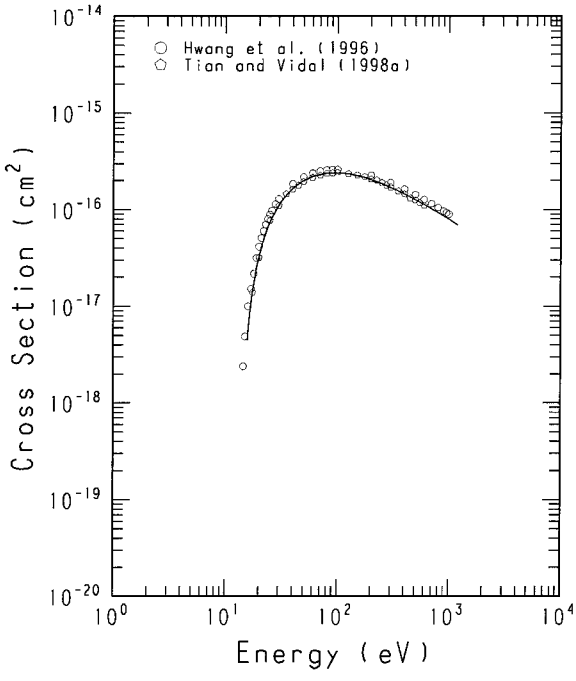

GRAPH 23

CO^+ Production/CO

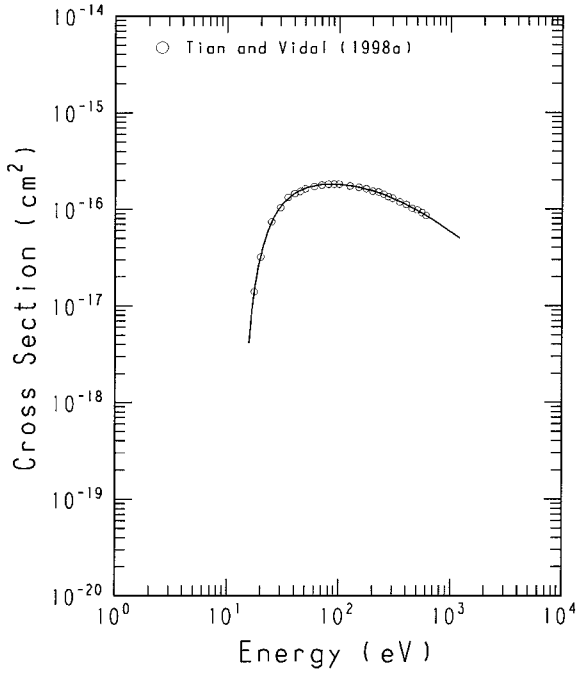

GRAPH 24

C^+ Production/CO

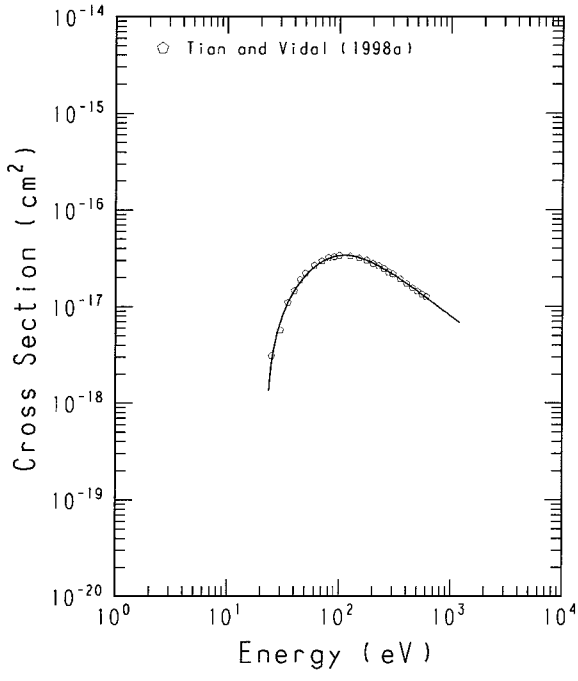

GRAPHS. Cross Section vs Electron Energy

See page 153 for Explanation of Graphs

GRAPH 25

O^+ production/CO

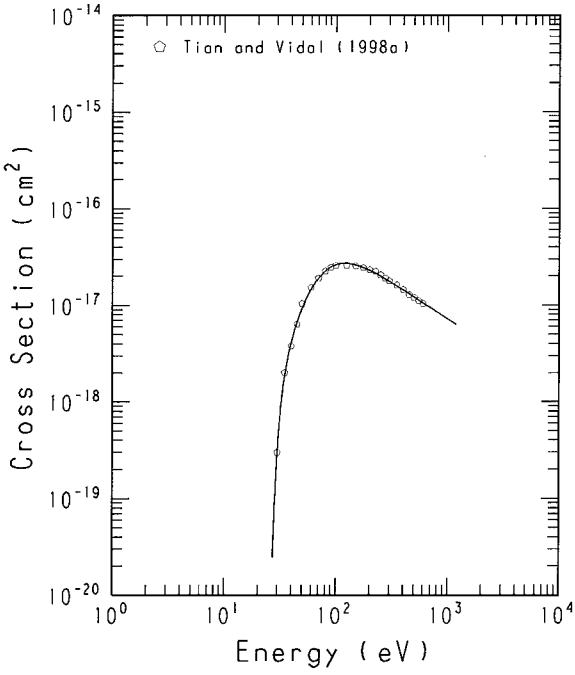

GRAPH 27

O^{2+} Production/CO

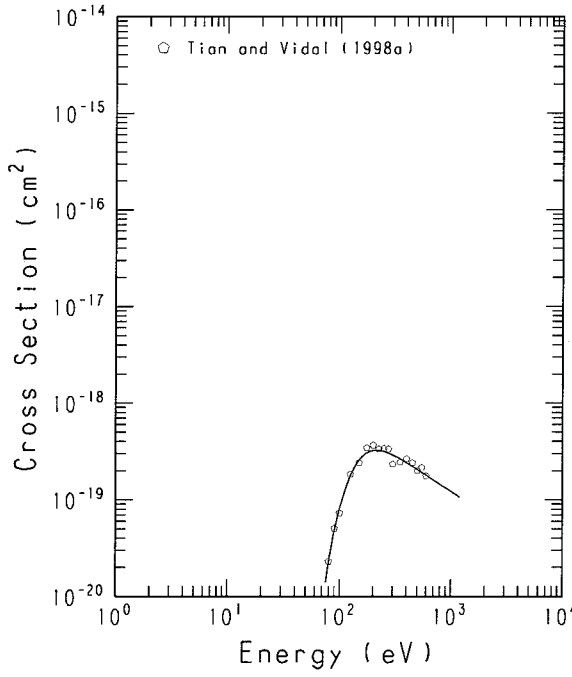

GRAPH 26

CO^{2+} Production/CO

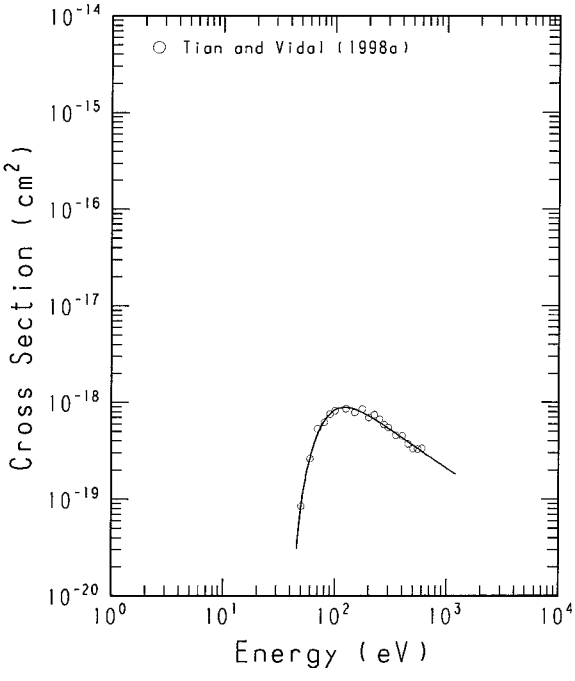

GRAPH 28

C^{2+} Production/CO

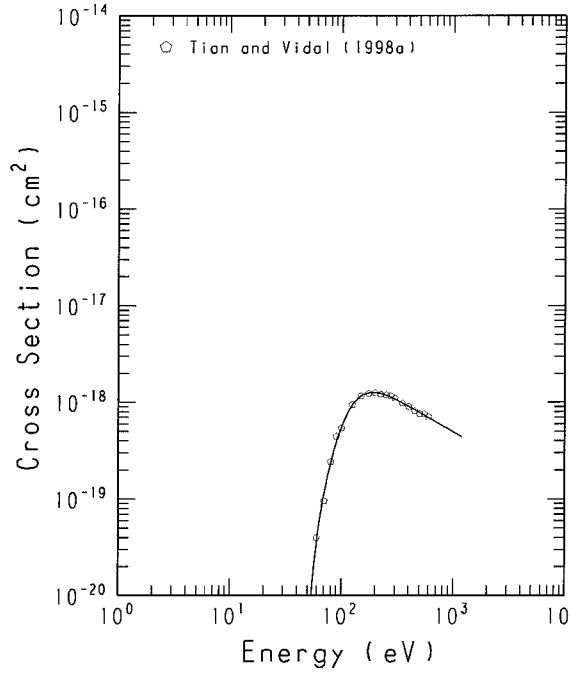

GRAPHS. Cross Section vs Electron Energy

See page 153 for Explanation of Graphs

GRAPH 29

Exc. to $CO^+(X\ ^2\Sigma^+)/CO$

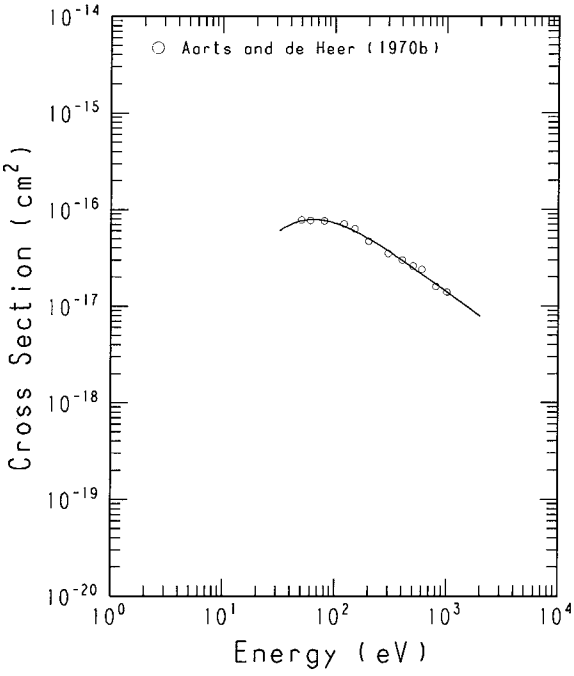

GRAPH 31

Exc. to $CO^+(B\ ^2\Sigma^+)/CO$

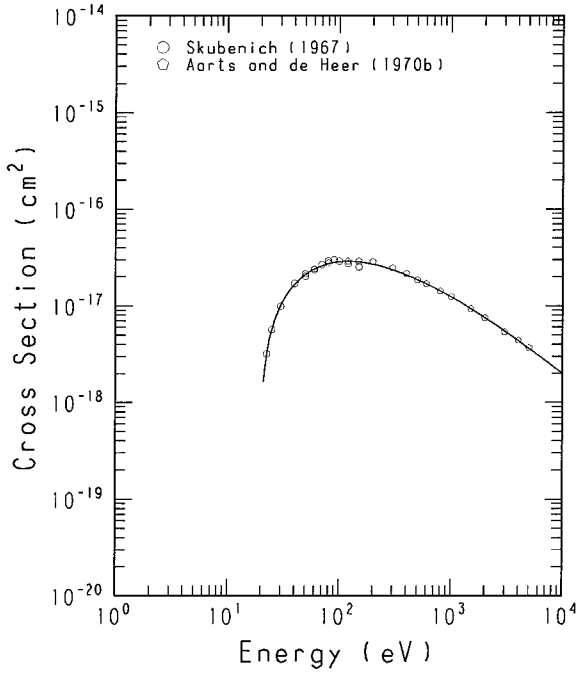

GRAPH 30

Exc. to $CO^+(A\ ^2\Pi)/CO$

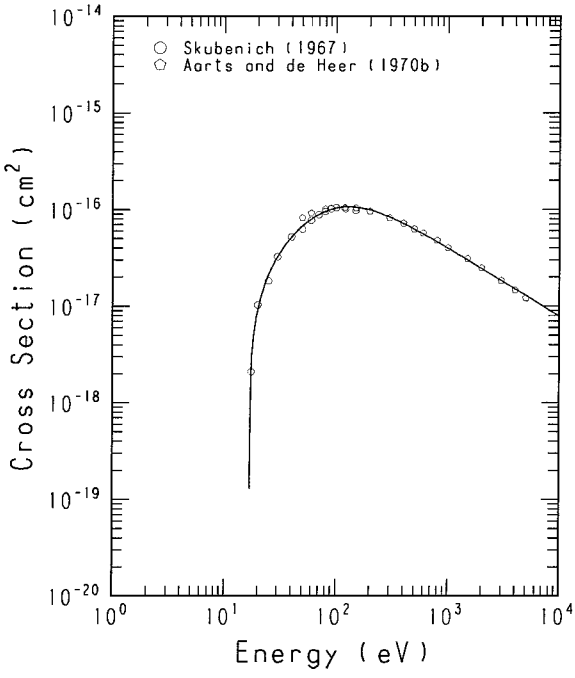

GRAPH 32

$CO^+(A\ ^2\Pi\text{-}X\ ^2\Sigma^+;v=3\text{-}0)/CO$ at 4011A

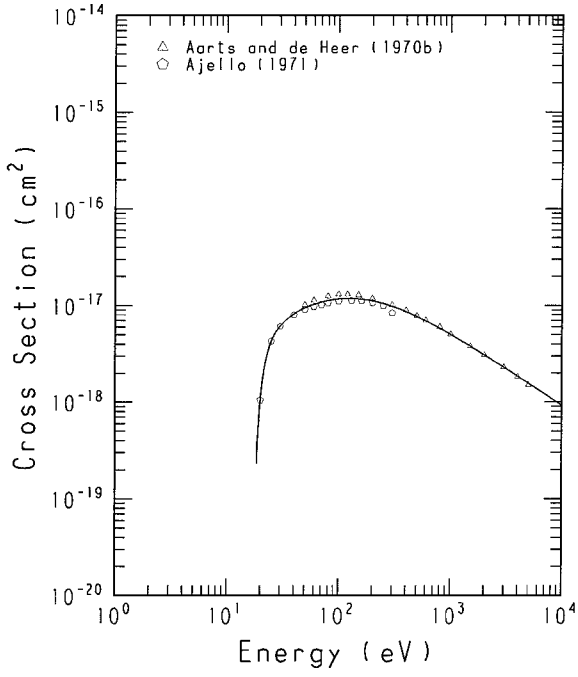

GRAPHS. Cross Section vs Electron Energy

See page 153 for Explanation of Graphs

GRAPH 33

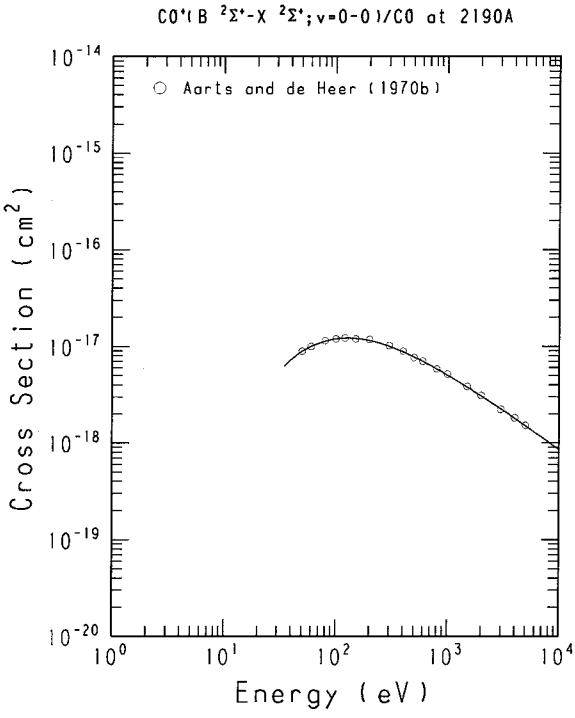

GRAPH 35

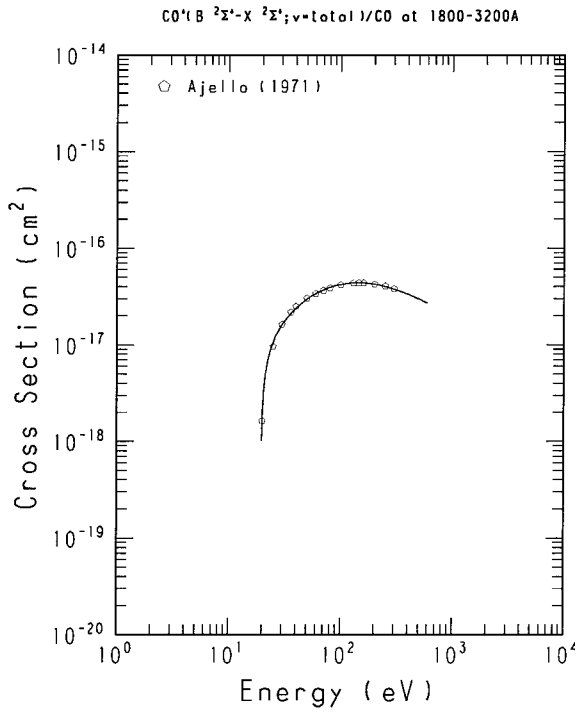

GRAPH 34

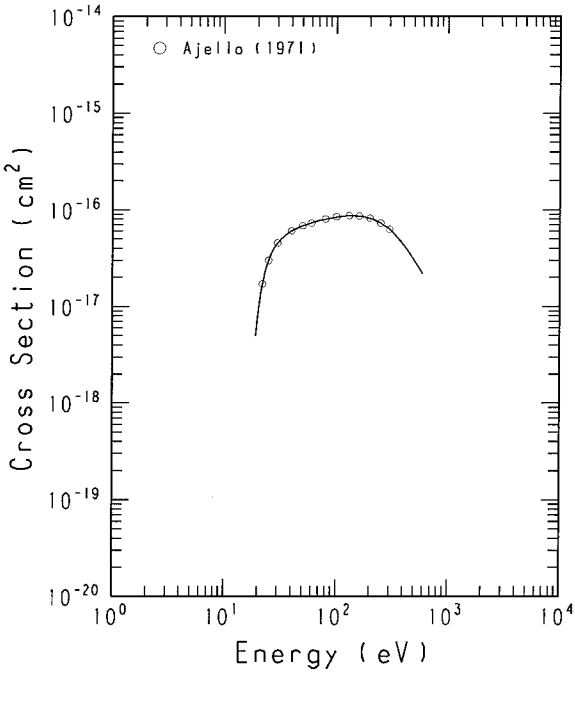

GRAPH 36

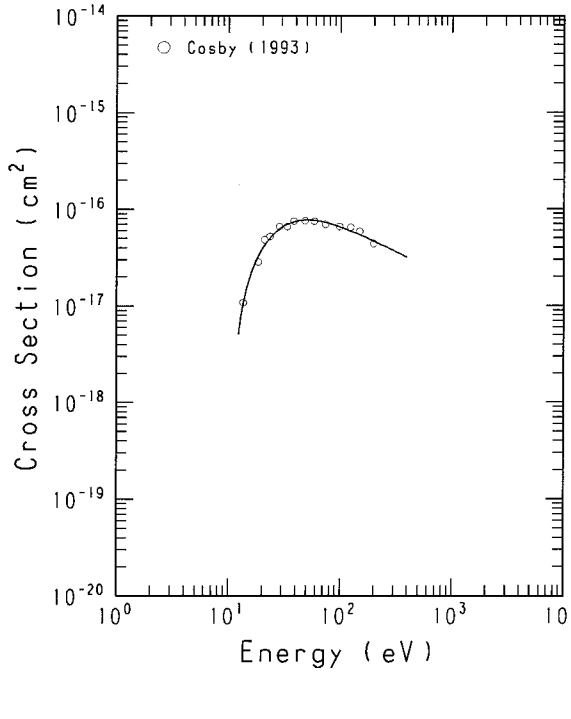

GRAPHS. Cross Section vs Electron Energy

See page 153 for Explanation of Graphs

GRAPH 37

O(^{1}S) Production/CO

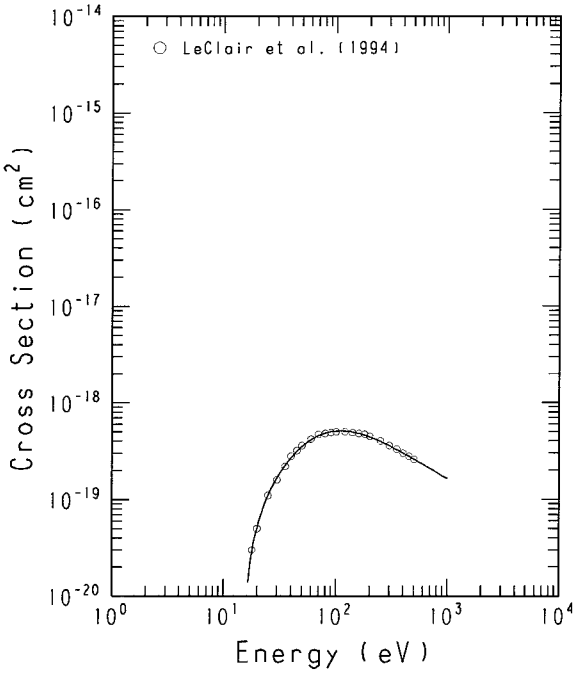

GRAPH 38

C I(3d,4s-2p)/CO at 1278-1280A

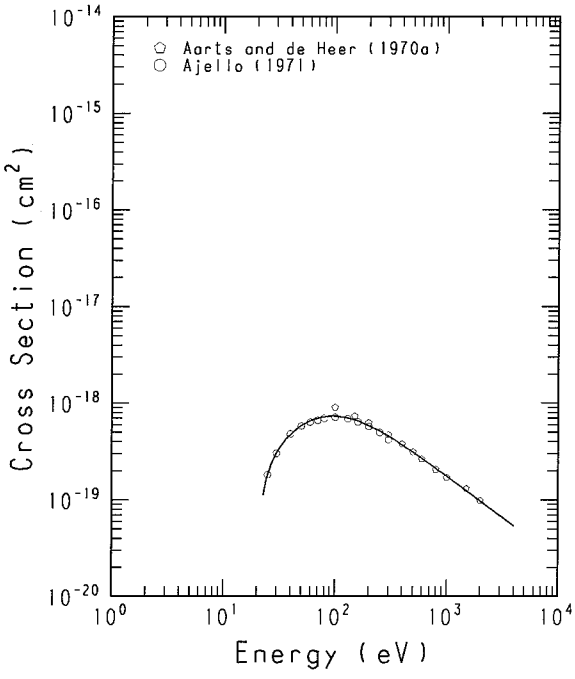

GRAPH 39

O I(^{3}S°-^{3}P)/CO_2 at 1304A

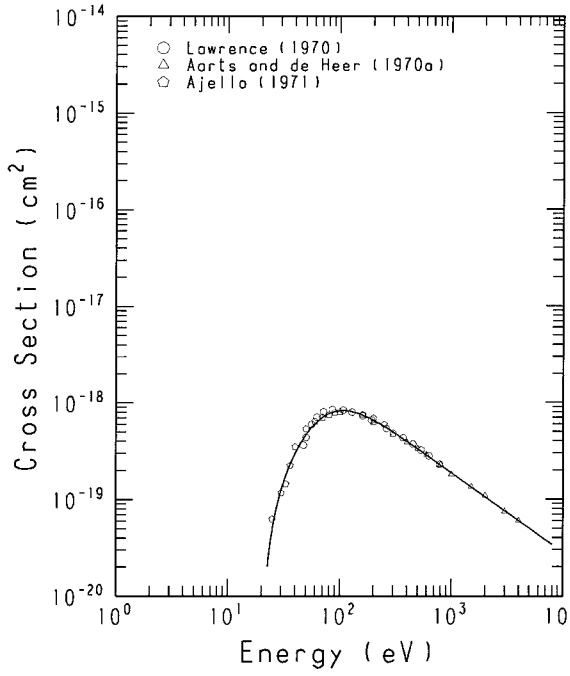

GRAPH 40

C II(^{2}D-^{2}P°)/CO at 1335A

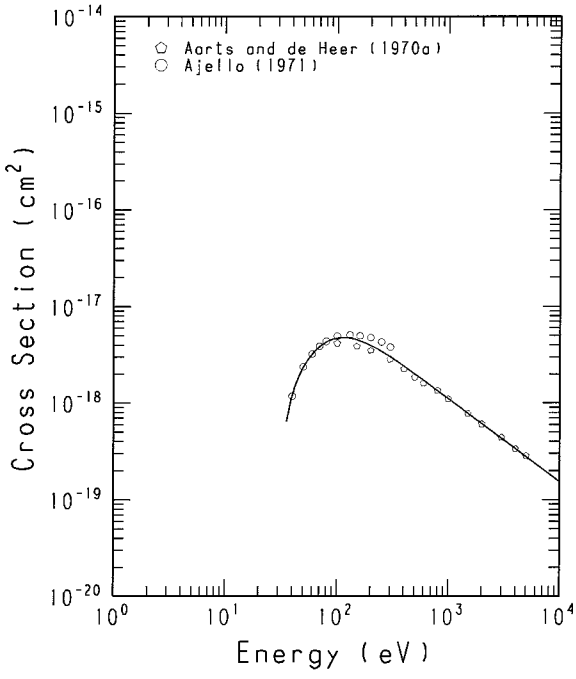

GRAPHS. Cross Section vs Electron Energy

See page 153 for Explanation of Graphs

GRAPH 41

O I(^3P-$^3S^o$)/CO at 8447A

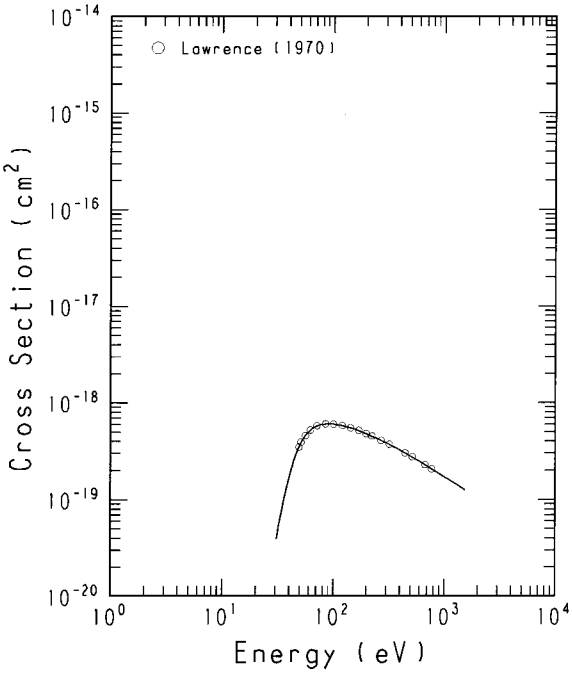

GRAPH 42

Total Scattering/CO_2

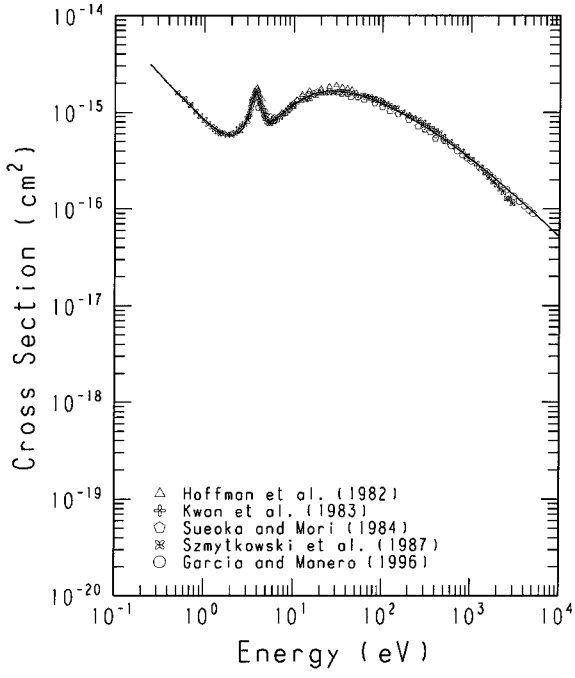

GRAPH 43

Elastic Scattering/CO_2

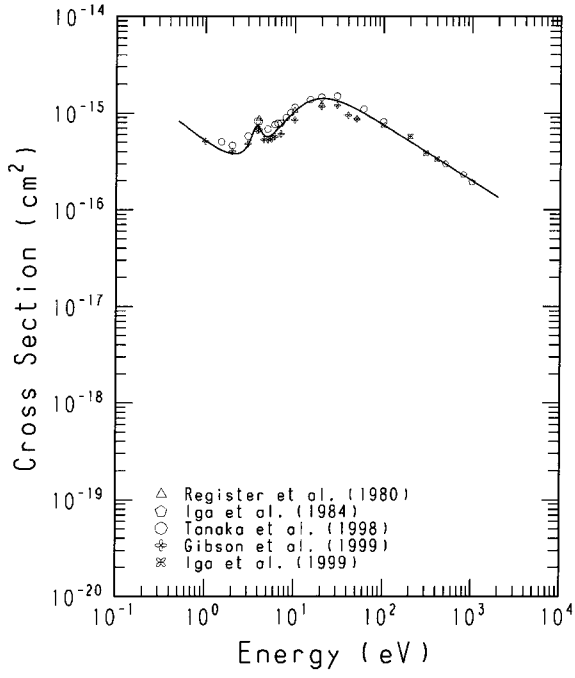

GRAPH 44

Momentum Transfer/CO_2

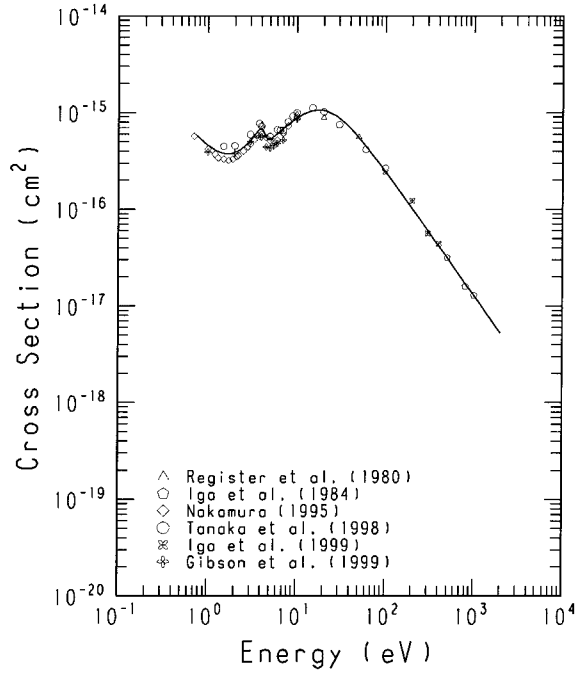

GRAPHS. Cross Section vs Electron Energy

See page 153 for Explanation of Graphs

GRAPH 45

Total Ionization/CO_2

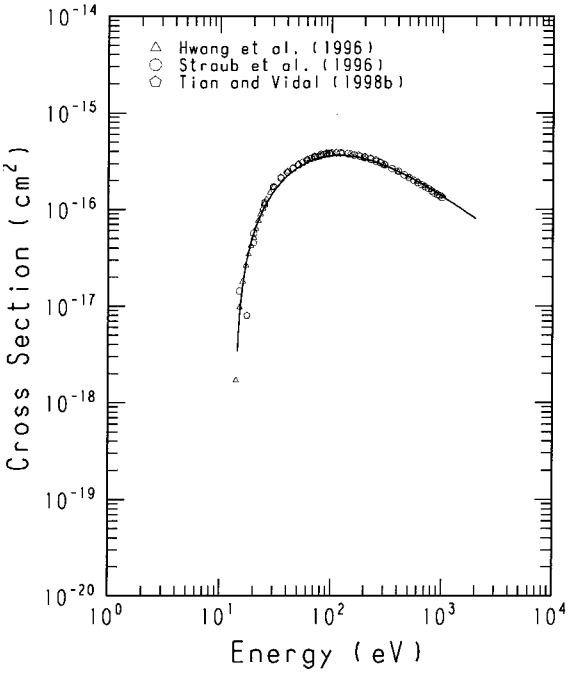

GRAPH 47

CO^+ Production/CO_2

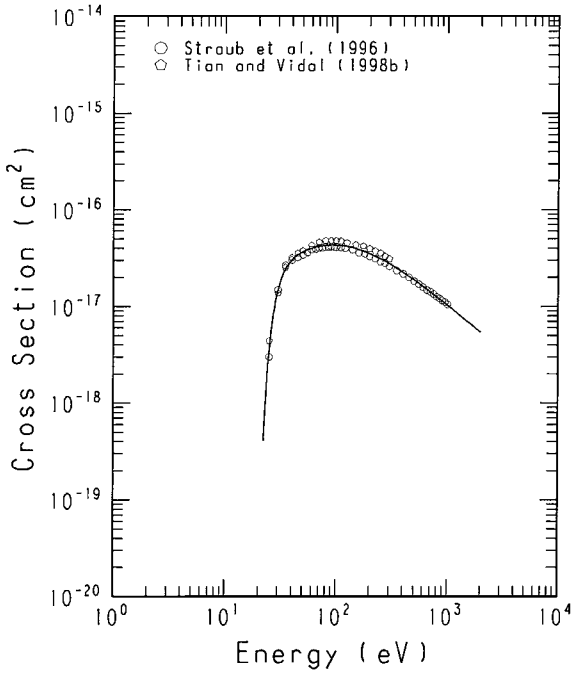

GRAPH 46

CO_2^+ Production/CO_2

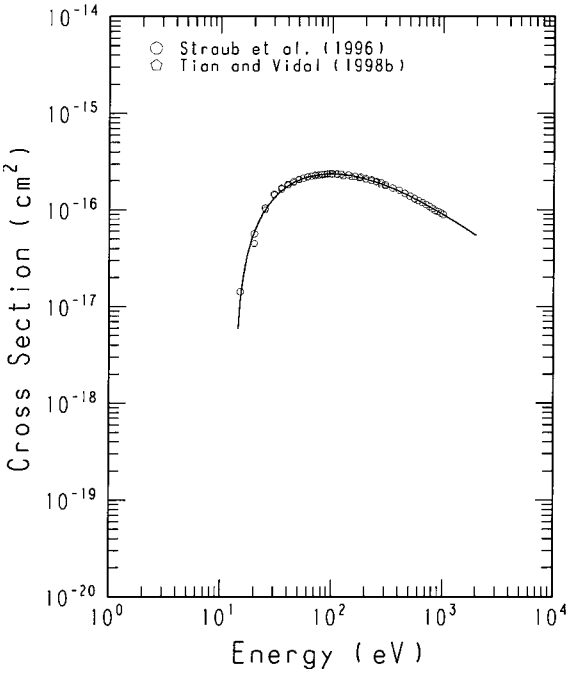

GRAPH 48

$CO^+ + O$ Production/CO_2

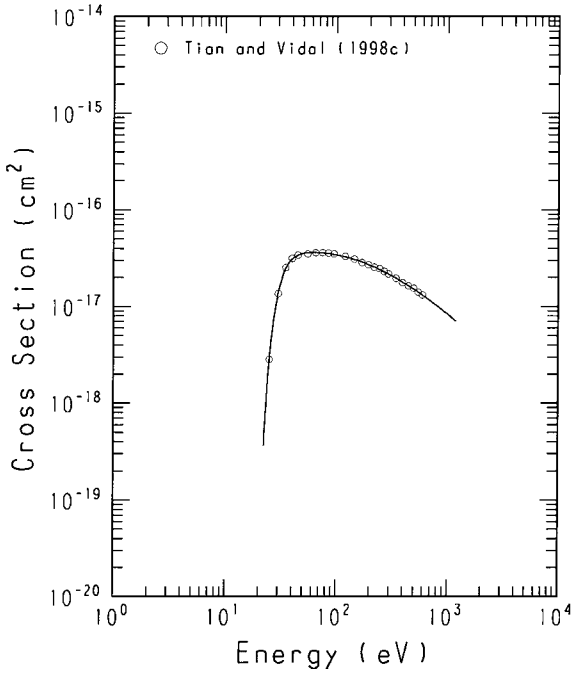

GRAPHS. Cross Section vs Electron Energy

See page 153 for Explanation of Graphs

GRAPH 49

O^+ Production/CO_2

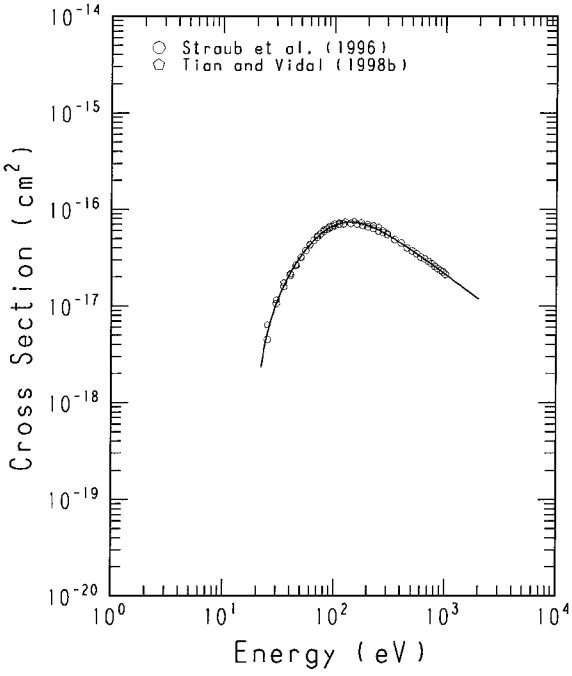

GRAPH 51

C^+ Production/CO_2

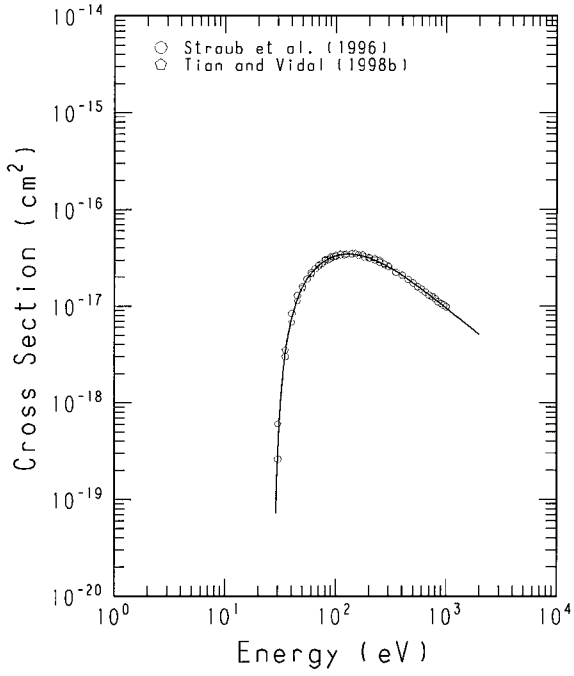

GRAPH 50

$O^+ + C + O$ Production/CO_2

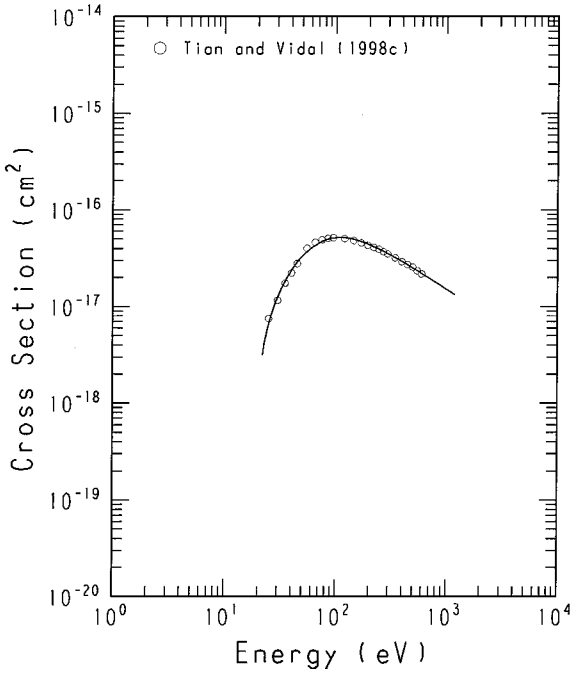

GRAPH 52

$C^+ + O + O$ Production/CO_2

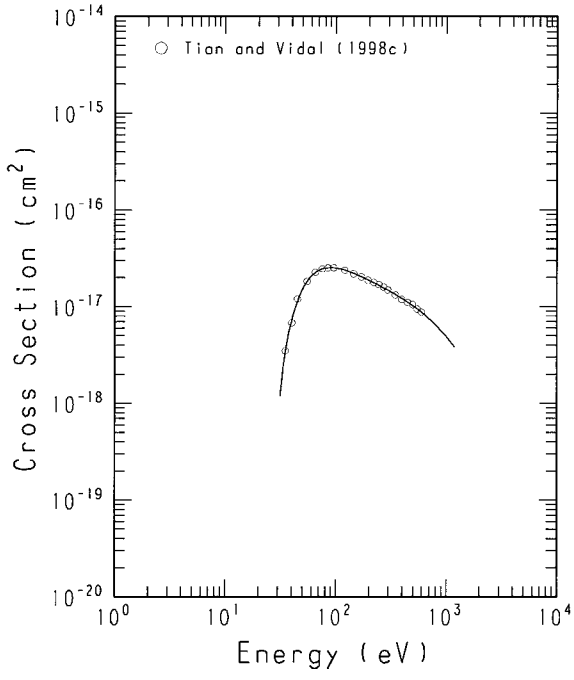

GRAPHS. Cross Section vs Electron Energy

See page 153 for Explanation of Graphs

GRAPH 53

CO_2^{2+} Production/CO_2

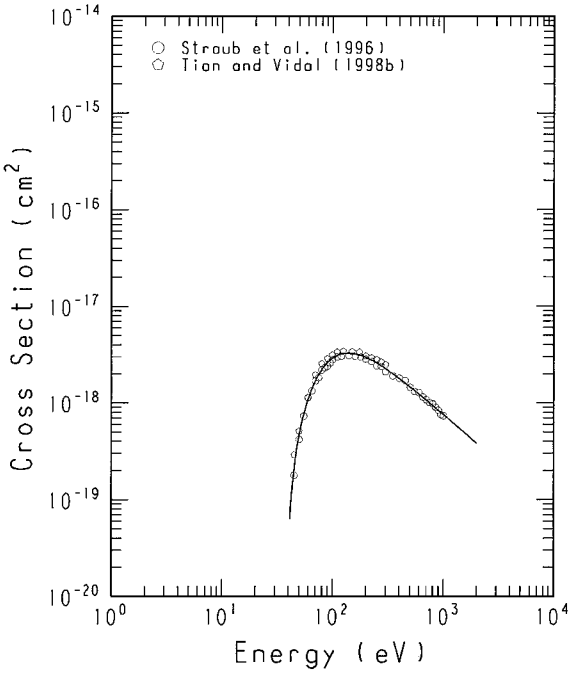

GRAPH 55

$O^+ + C$ Production/CO_2

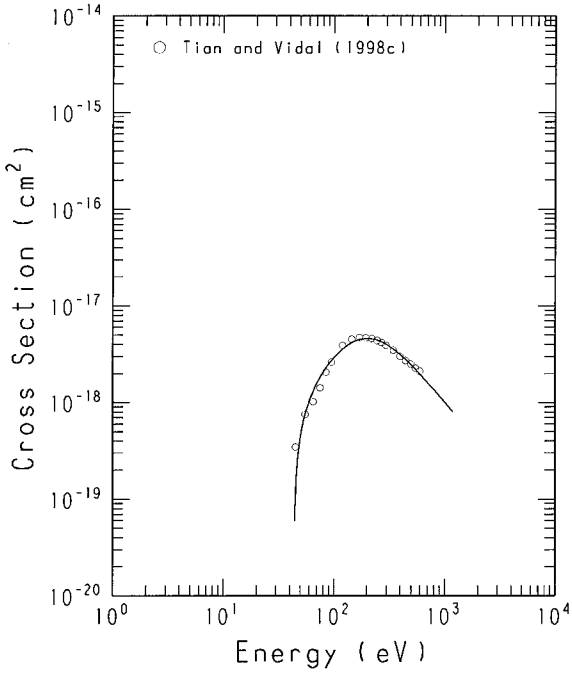

GRAPH 54

$O^+ + CO^+$ Production/CO_2

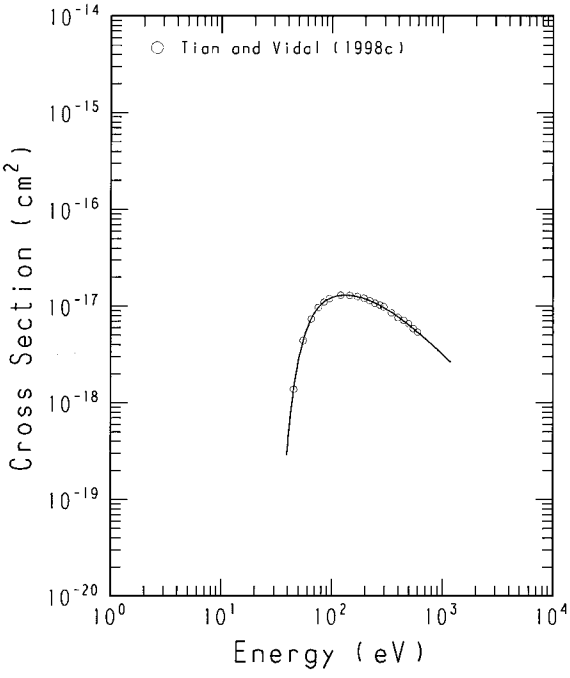

GRAPH 56

$C^+ + O^+ + O$ Production/CO_2

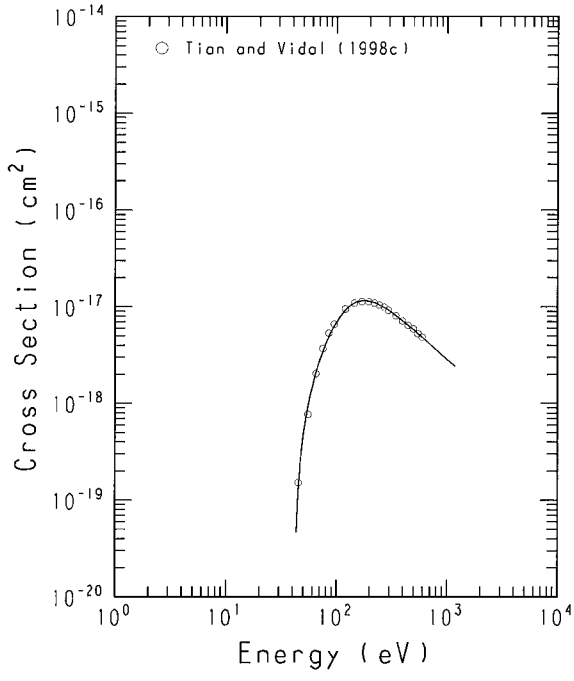

GRAPHS. Cross Section vs Electron Energy

See page 153 for Explanation of Graphs

GRAPH 57

O^{2+} Production/CO_2

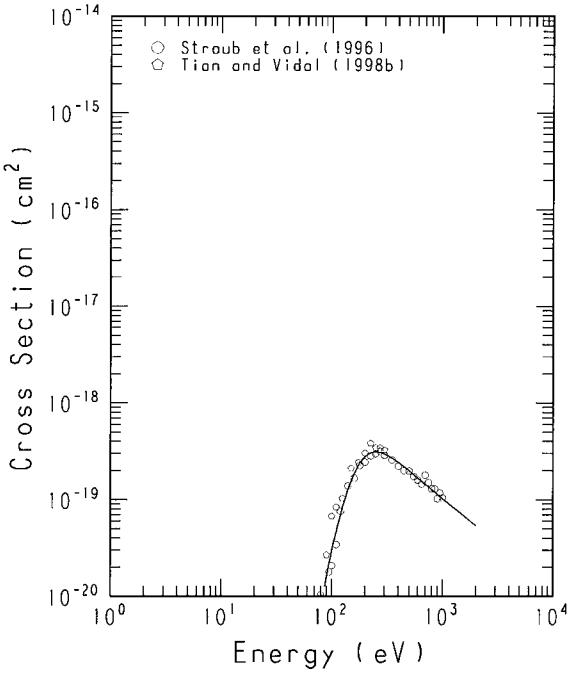

GRAPH 58

C^{2+} Production/CO_2

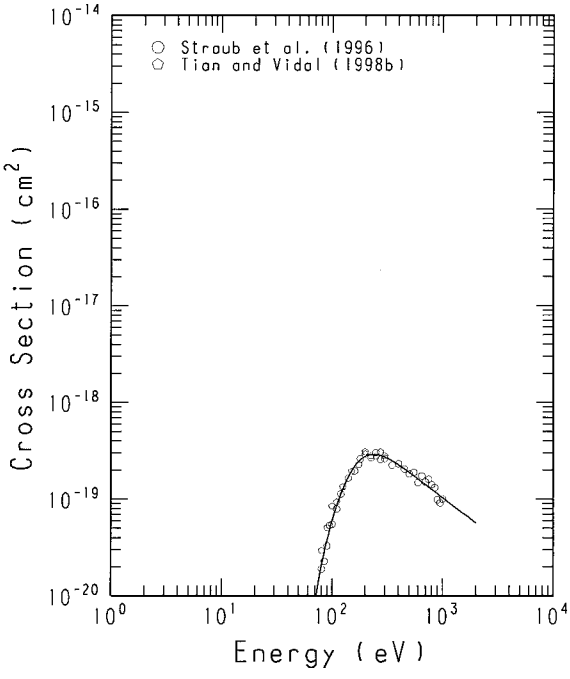

GRAPH 59

$CO_2^+(A\ ^2\Pi_u - X\ ^2\Pi_g; v=total)/CO_2$ at 2930-4390A

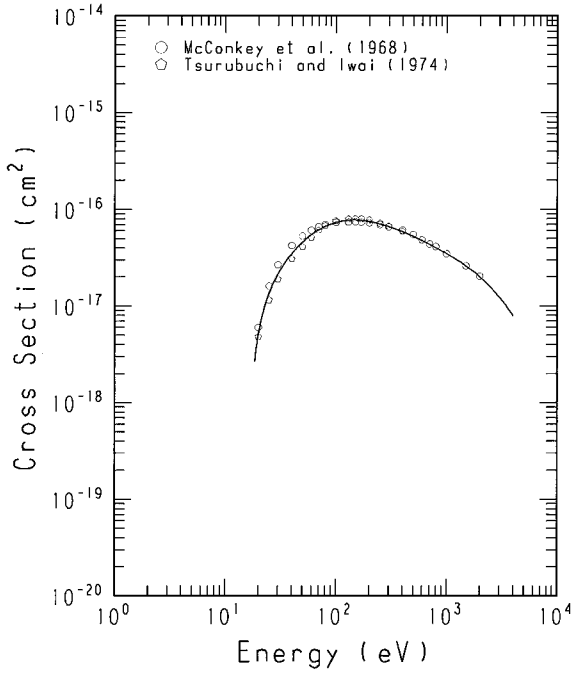

GRAPH 60

$CO_2^+(B\ ^2\Sigma_u^+ - X\ ^2\Pi_g; v=total)/CO_2$ at 2880-2900A

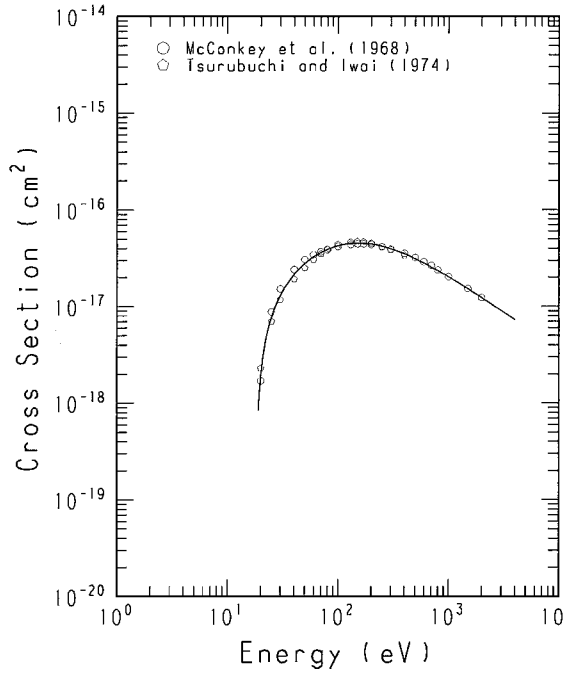

GRAPHS. Cross Section vs Electron Energy

See page 153 for Explanation of Graphs

GRAPH 61

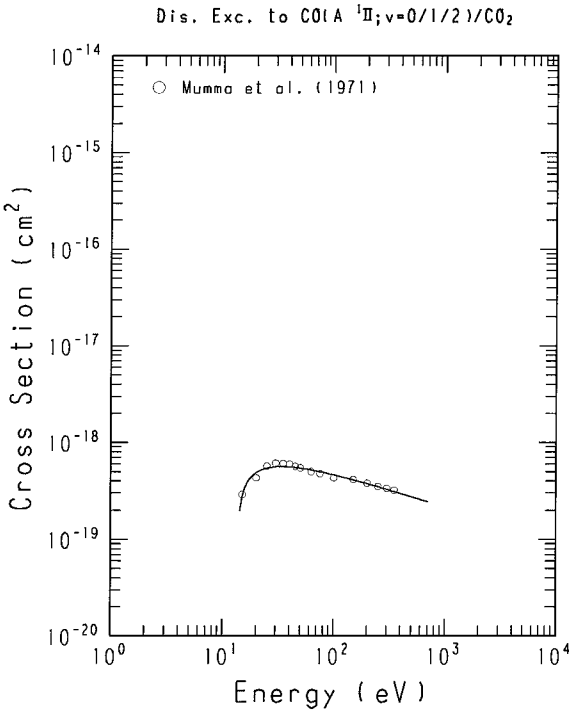

GRAPH 62

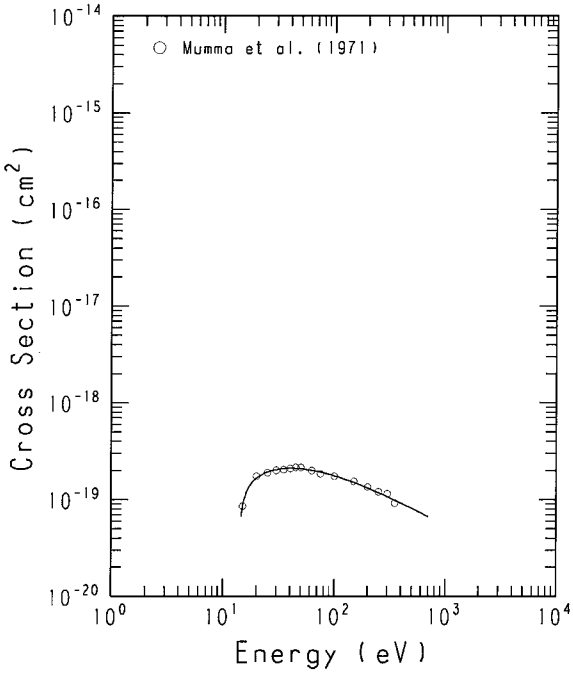

GRAPH 63

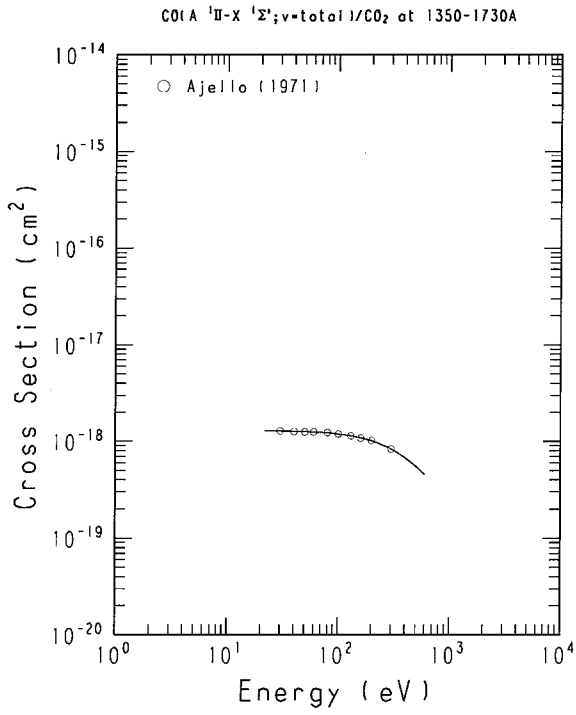

GRAPH 64

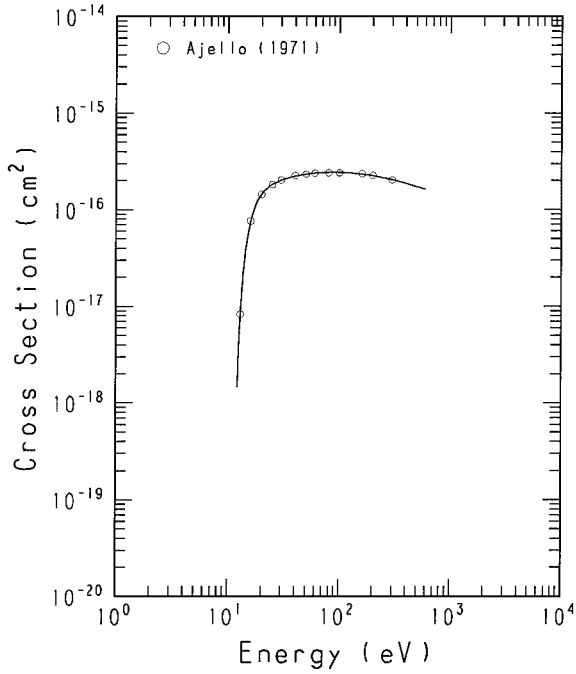

GRAPHS. Cross Section vs Electron Energy

See page 153 for Explanation of Graphs

GRAPH 65

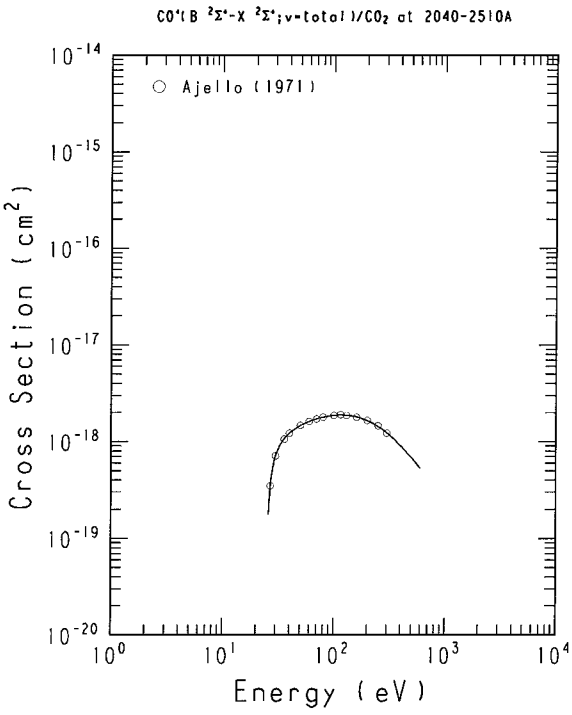

GRAPH 67

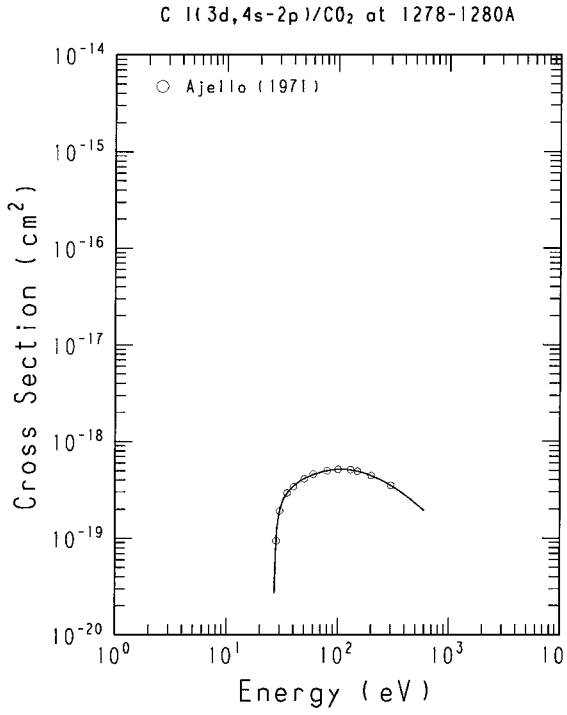

GRAPH 66

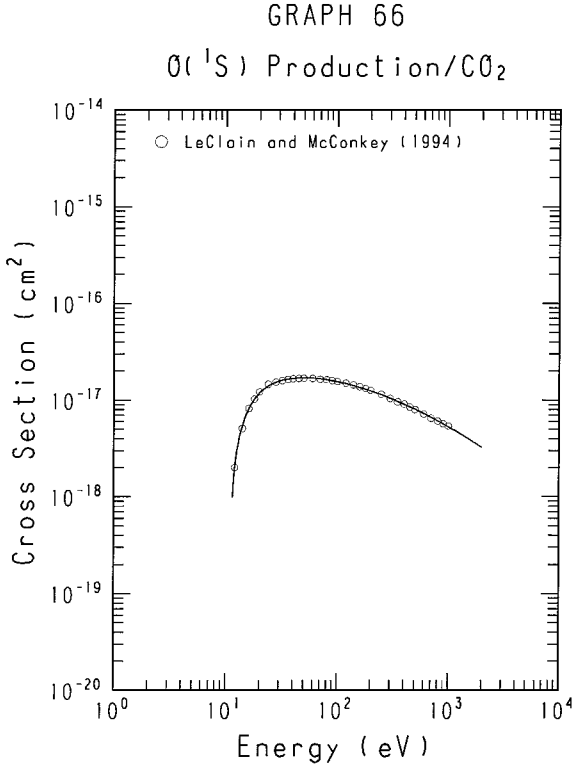

GRAPH 68

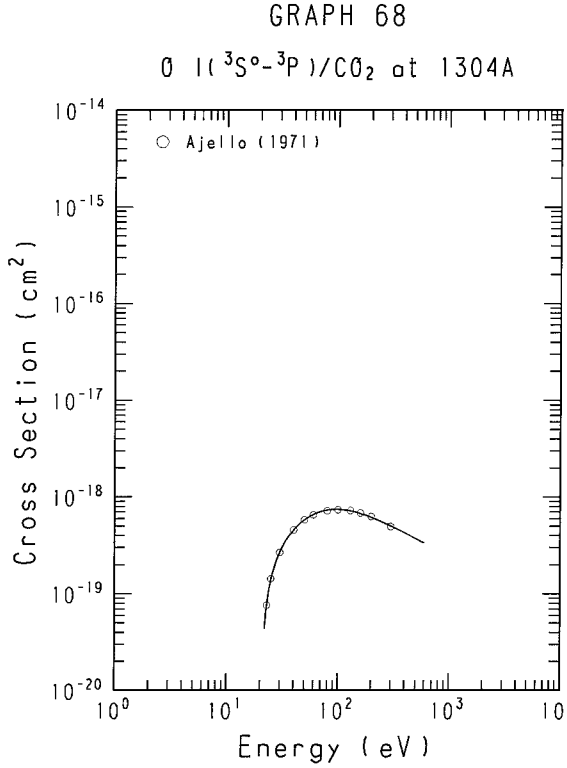

GRAPHS. Cross Section vs Electron Energy

See page 153 for Explanation of Graphs

GRAPH 69

C II(^{2}D-^{2}P°)/CO_2 at 1335A

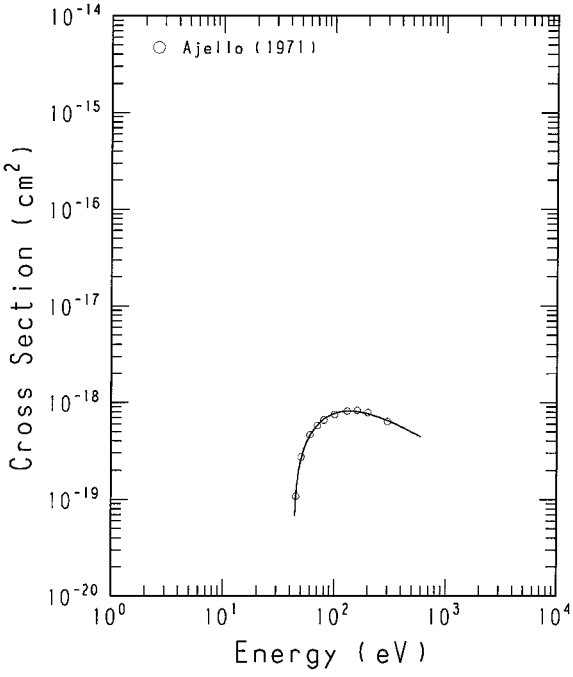

GRAPH 70

Total Scattering/H_2O

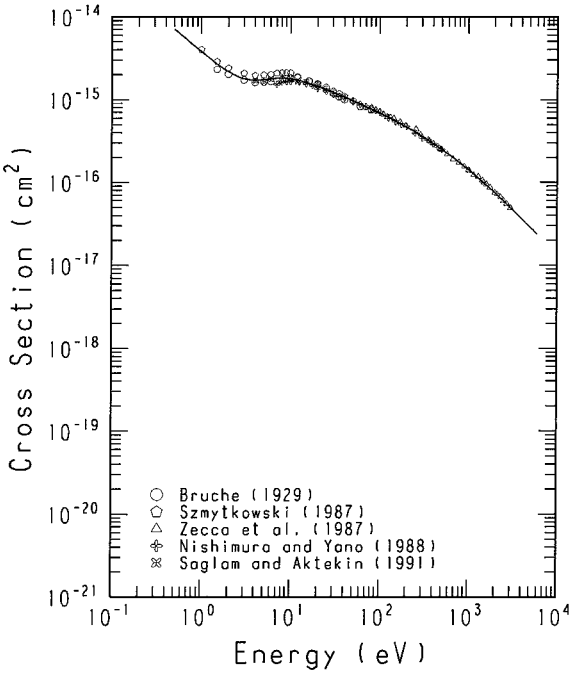

GRAPH 71

Elastic Scattering/H_2O

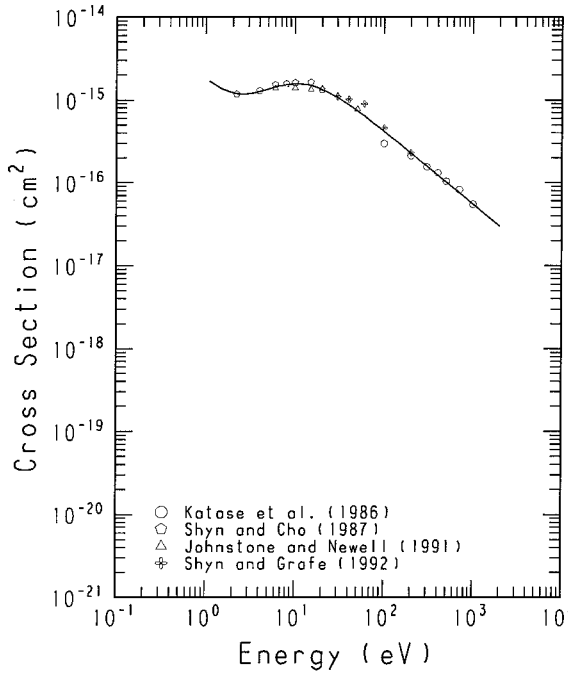

GRAPH 72

Momentum Transfer/H_2O

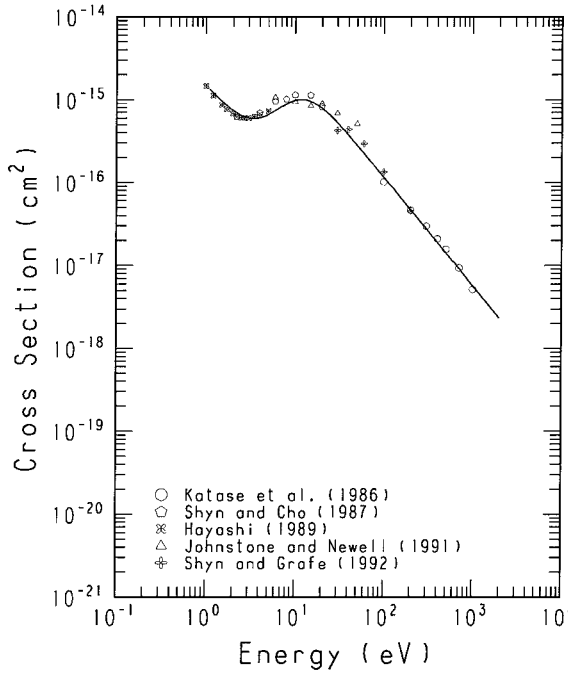

GRAPHS. Cross Section vs Electron Energy

See page 153 for Explanation of Graphs

GRAPH 73

Vib. Exc. (Bending)/H_2O

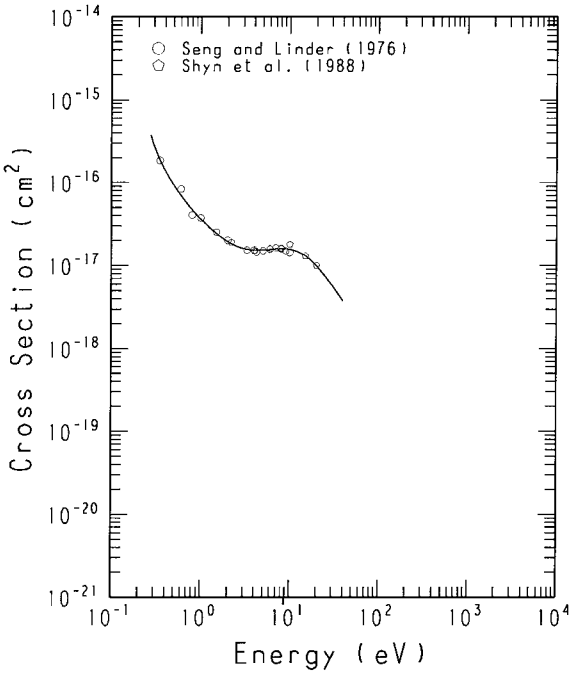

GRAPH 74

Vib. Exc. (Stretching)/H_2O

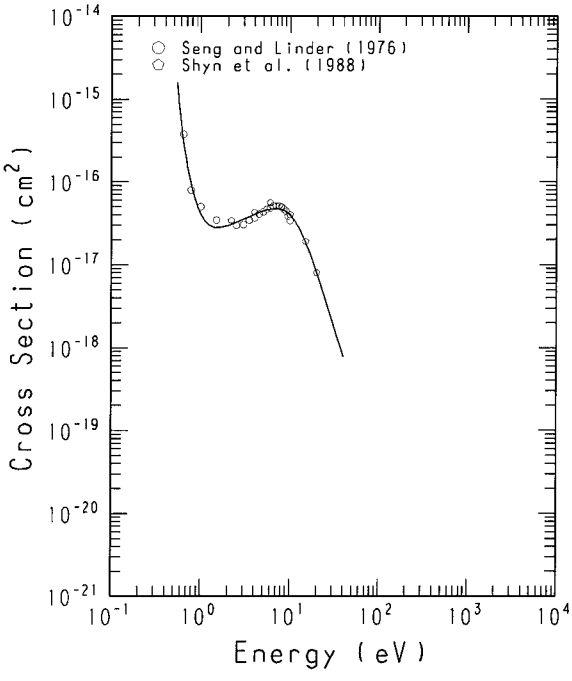

GRAPH 75

Total Ionization/H_2O

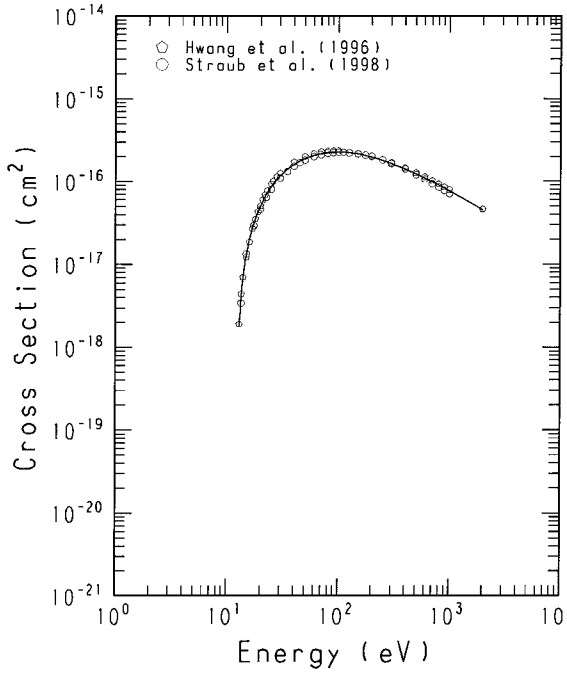

GRAPH 76

H_2O^+ Production/H_2O

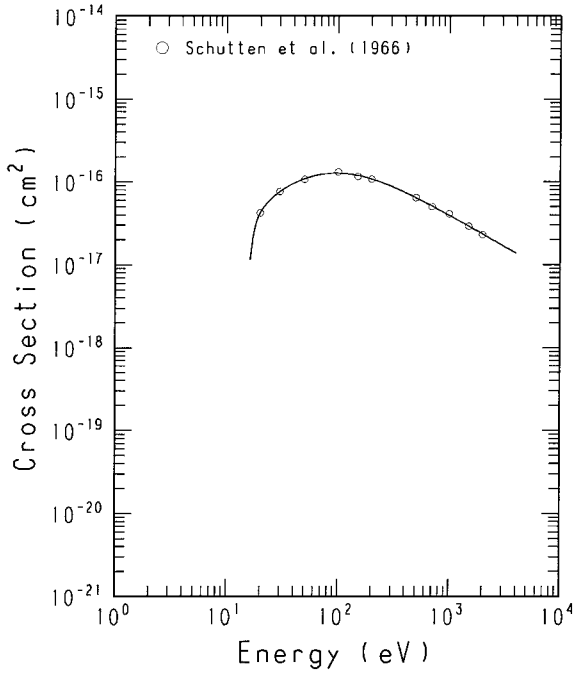

GRAPHS. Cross Section vs Electron Energy

See page 153 for Explanation of Graphs

GRAPH 77

OH^+ Production/H_2O

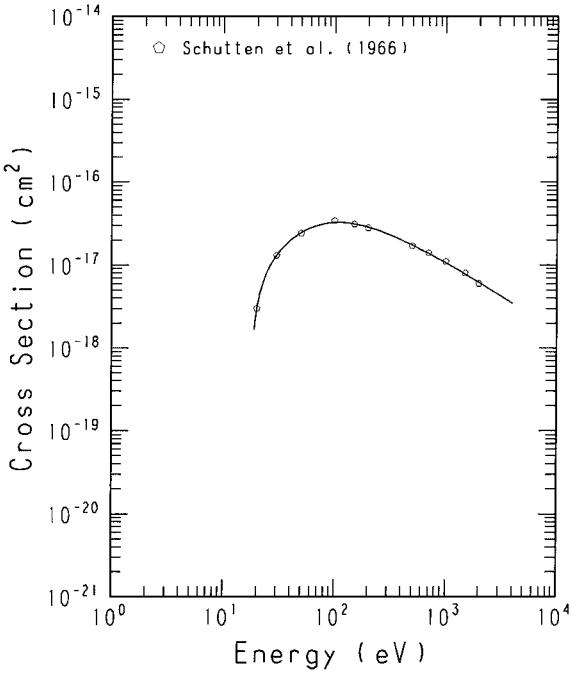

GRAPH 79

O^{2+} Production/H_2O

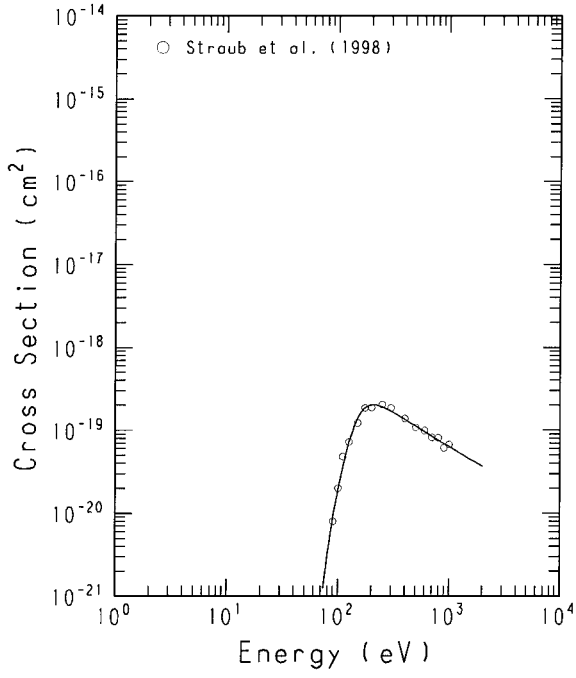

GRAPH 78

O^+ Production/H_2O

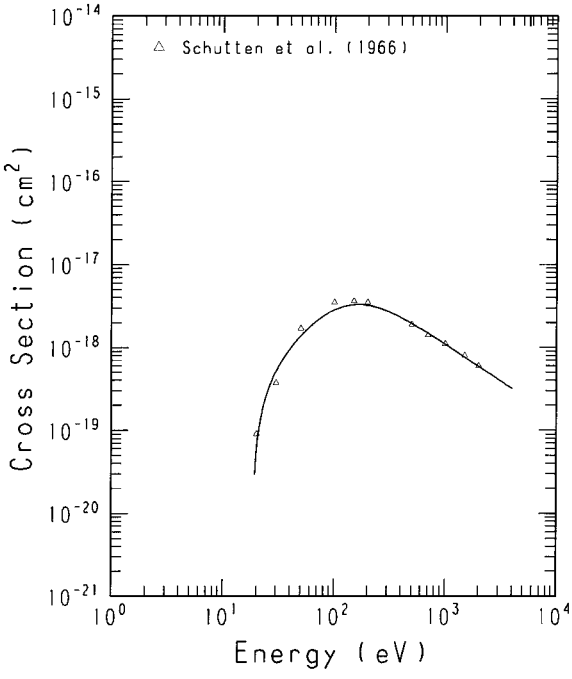

GRAPH 80

H_2^+ Production/H_2O

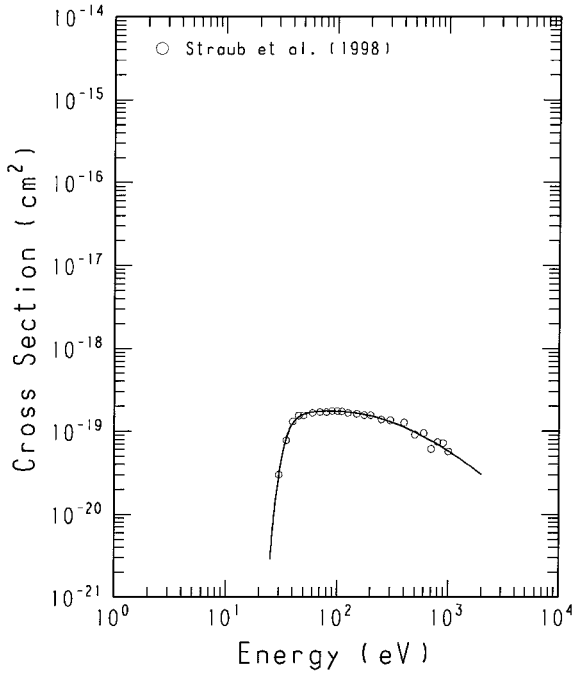

GRAPHS. Cross Section vs Electron Energy

See page 153 for Explanation of Graphs

GRAPH 81

H^+ Production/H_2O

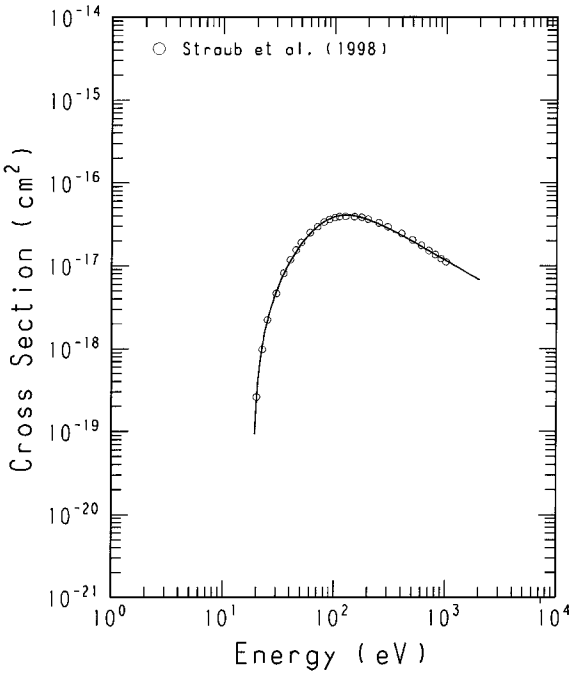

GRAPH 83

H(n=4) Production/H_2O

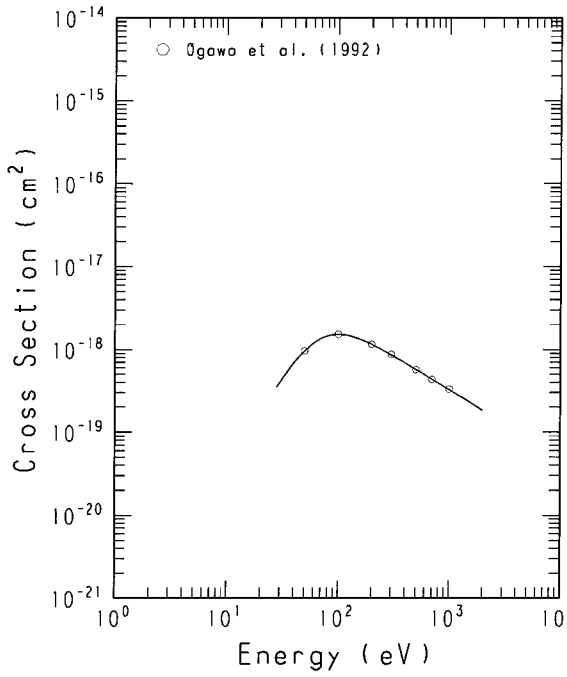

GRAPH 82

H(n=3) Production/H_2O

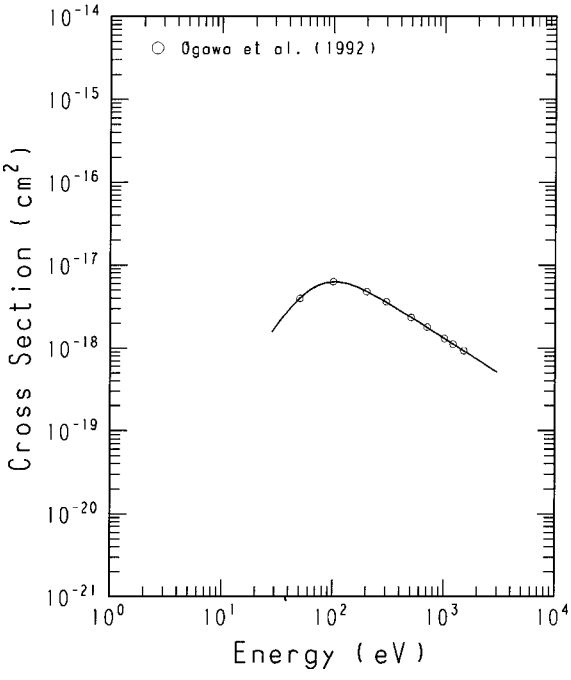

GRAPH 84

Lyman-α/H_2O

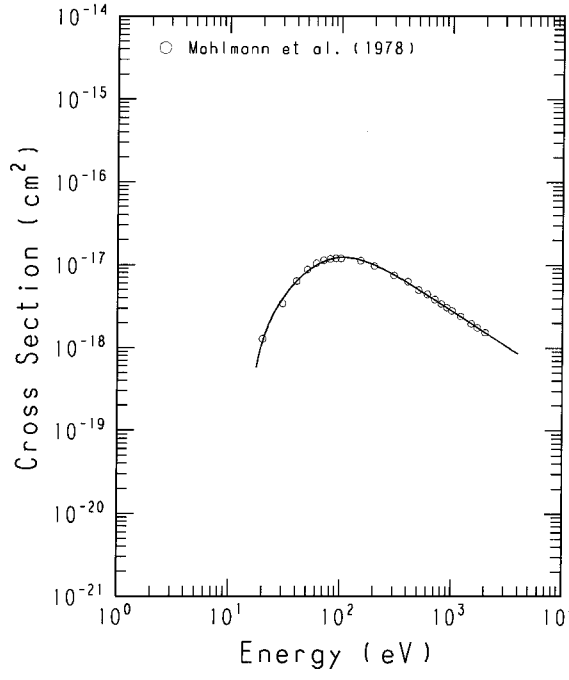

GRAPHS. Cross Section vs Electron Energy

See page 153 for Explanation of Graphs

GRAPH 85

Balmer-α/H_2O

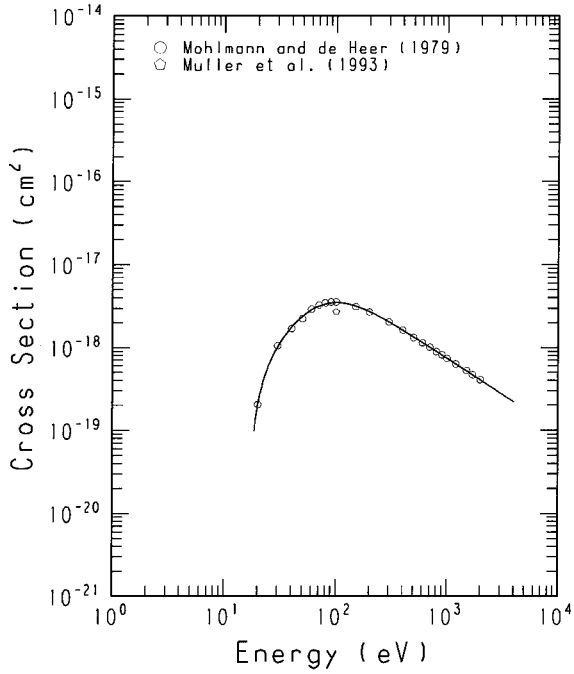

GRAPH 87

Balmer-γ/H_2O

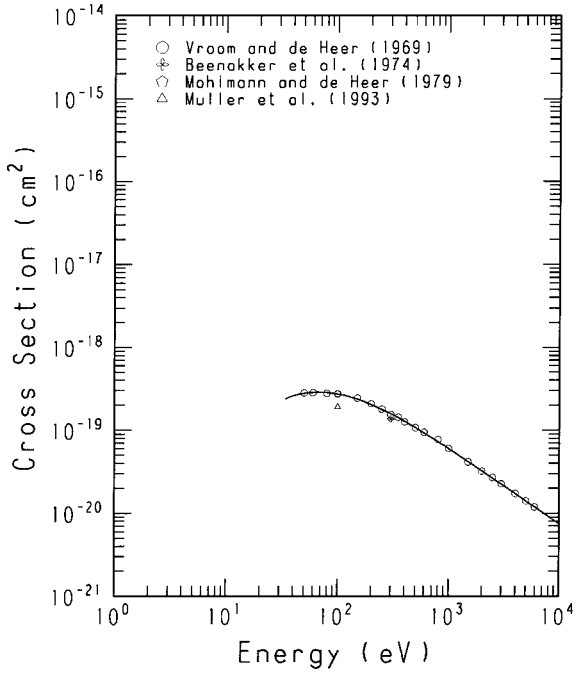

GRAPH 86

Balmer-β/H_2O

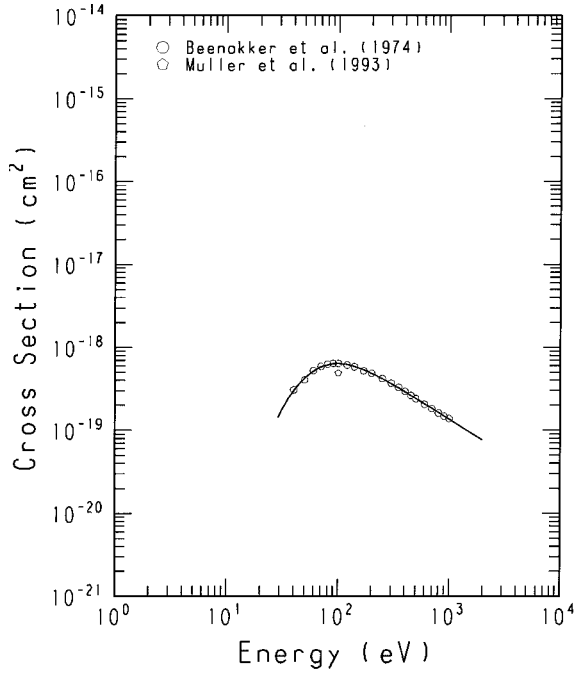

GRAPH 88

Balmer-δ/H_2O

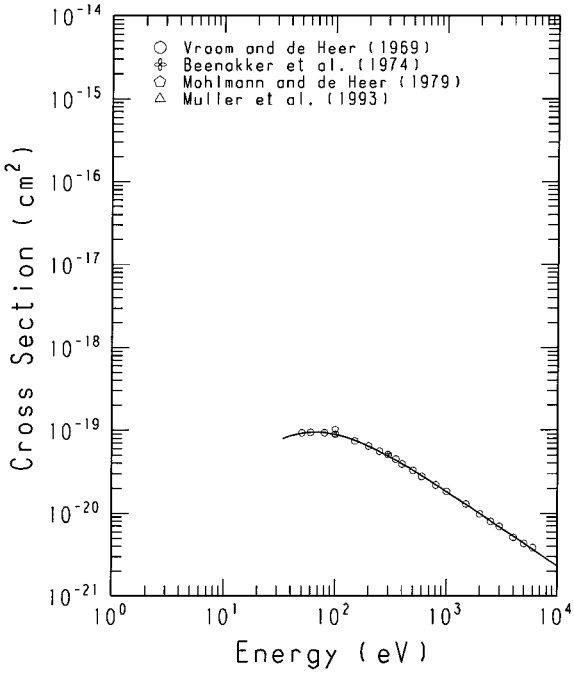

GRAPHS. Cross Section vs Electron Energy

See page 153 for Explanation of Graphs

GRAPH 89

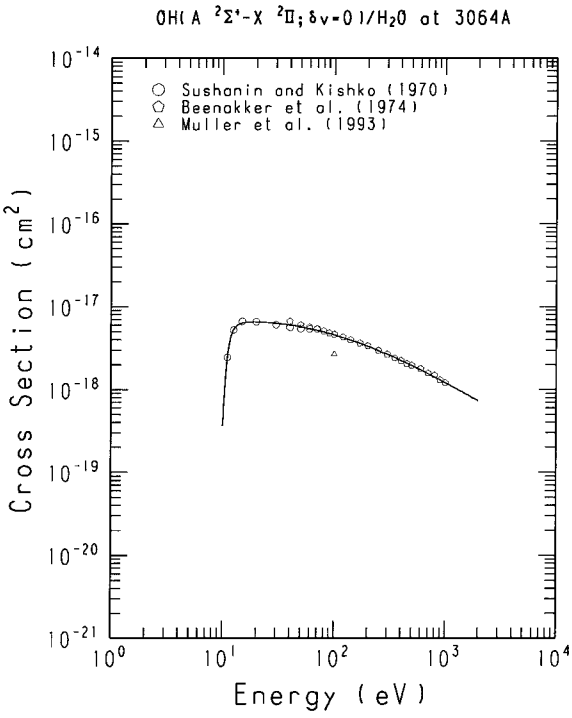

GRAPH 91

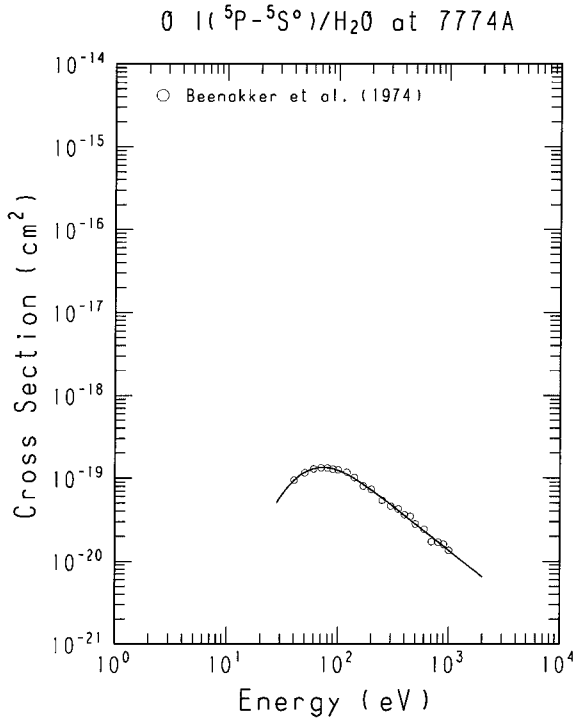

GRAPH 90

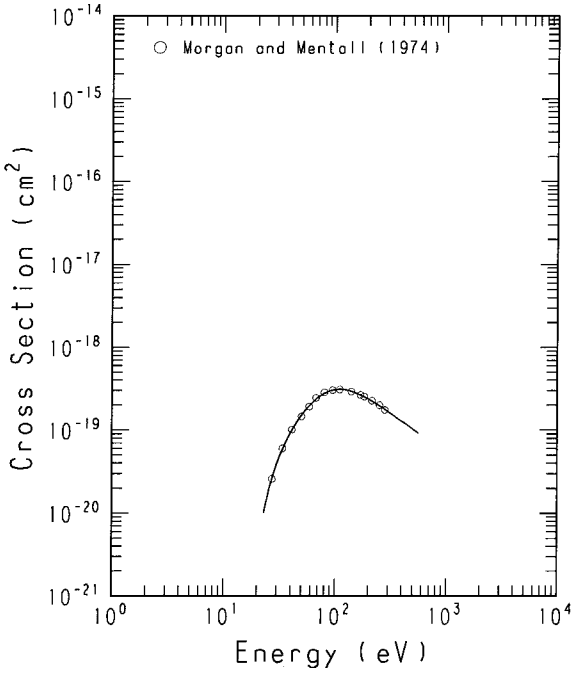

GRAPH 92